Human Molecular Genetics, 2015, Vol. 24, No. 1 **213–229**
doi:10.1093/hmg/ddu440
Advance Access published on August 28, 2014

Junctophilin-1 is a modifier gene of *GDAP1*-related Charcot–Marie–Tooth disease

David Pla-Martín[1,2,†], Eduardo Calpena[1,2,†], Vincenzo Lupo[1,2], Celedonio Márquez[3], Eloy Rivas[4], Rafael Sivera[5,6], Teresa Sevilla[5,6,7], Francesc Palau[1,2,9,†] and Carmen Espinós[1,2,8,†,*]

[1]Program in Rare and Genetic Diseases and IBV/CSIC Associated Unit, Centro de Investigación Príncipe Felipe (CIPF), Valencia 46012, Spain, [2]Centro de Investigación Biomédica en Red de Enfermedades Raras (CIBERER), Valencia 46012, Spain, [3]Department of Neurology and , [4]Department of Pathology, Hospital Universitario Virgen del Rocío, Seville 41013, Spain, [5]Department of Neurology, Hospital Universitari i Politècnic La Fe and Instituto de Investigación Sanitario (IIS)—La Fe, Valencia 46026, Spain, [6]Centro de Investigación Biomédica en Red de Enfermedades Neurodegenerativas (CIBERNED), Valencia 46026, Spain, [7]Department of Medicine and [8]Department of Genetics, Universitat de València, Valencia 46010, Spain and [9]University of Castilla-La Mancha School of Medicine, Ciudad Real 13071, Spain

Received July 8, 2014; Revised August 21, 2014; Accepted August 22, 2014

Mutations in the *GDAP1* gene cause different forms of Charcot–Marie–Tooth (CMT) disease, and the primary clinical expression of this disease is markedly variable in the dominant inheritance form (CMT type 2K; CMT2K), in which carriers of the *GDAP1* p.R120W mutation can display a wide range of clinical severity. We investigated the *JPH1* gene as a genetic modifier of clinical expression variability because junctophilin-1 (JPH1) is a good positional and functional candidate. We demonstrated that the *JPH1-GDAP1* cluster forms a paralogon and is conserved in vertebrates. Moreover, both proteins play a role in Ca^{2+} homeostasis, and we demonstrated that JPH1 is able to restore the store-operated Ca^{2+} entry (SOCE) activity in *GDAP1*-silenced cells. After the mutational screening of *JPH1* in a series of 24 CMT2K subjects who harbour the *GDAP1* p.R120W mutation, we characterized the *JPH1* p.R213P mutation in one patient with a more severe clinical picture. $JPH1^{p.R213P}$ cannot rescue the SOCE response in *GDAP1*-silenced cells. We observed that JPH1 colocalizes with STIM1, which is the activator of SOCE, in endoplasmic reticulum-plasma membrane puncta structures during Ca^{2+} release in a *GDAP1*-dependent manner. However, when $GDAP1^{p.R120W}$ is expressed, JPH1 seems to be retained in mitochondria. We also established that the combination of $GDAP1^{p.R120W}$ and $JPH1^{p.R213P}$ dramatically reduces SOCE activity, mimicking the effect observed in *GDAP1* knock-down cells. In summary, we conclude that JPH1 and GDAP1 share a common pathway and depend on each other; therefore, *JPH1* can contribute to the phenotypical consequences of *GDAP1* mutations.

INTRODUCTION

The most reliable and predictive factor of genetic disease is the nature of the mutation responsible for the phenotype. Quite often, correlating the phenotype to the genotype is complicated by the complex interactions of the environment with other primarily unidentified genetic factors. Mutations in the *ganglioside-induced differentiation-associated protein 1* (*GDAP1*) gene cause different forms of Charcot–Marie–Tooth (CMT) disease: autosomal recessive demyelinating [Charcot–Marie–Tooth type 4A (CMT4A), MIM 214400] (1), axonal [autosomal recessive Charcot–Marie–Tooth type 2K (AR-CMT2K), MIM 607831] (2), intermediate [recessive intermediate Charcot–Marie–Tooth type A (RI-CMTA), MIM 608340] (3,4) and autosomal dominant axonal [Charcot–Marie–Tooth type 2K (CMT2K), MIM 607831] (5). The clinical picture of CMT2K patients presents a mild-to-moderate phenotype, and although incomplete penetrance is generally rare in the context of CMT, this possibility is not uncommon in autosomal dominant *GDAP1*-associated neuropathies (6,7). Observing the presence of asymptomatic individuals who have an affected parent, affected children, or both, and individuals with the same pathological mutation who show wide clinical variability is common.

*To whom correspondence should be addressed at: Centro de Investigación Príncipe Felipe (CIPF), Unit of Genetics and Genomics of Neuromuscular Diseases, c/Eduardo Primo Yúfera, 3, 46012 Valencia, Spain. Tel: +34 963 289 680; Fax: +34 963 289 701; Email: cespinos@cipf.es
†These authors contributed equally to this work.

The *GDAP1* gene maps on chromosome 8q21.1 (chromosome 8: 75,233,365–75,401,107; forward strand) and encodes a protein belonging to a glutathione *S*-transferase enzyme subfamily (8). GDAP1 is an outer mitochondrial membrane protein, where this protein acts as a regulator of mitochondrial dynamics (9,10), and is primarily expressed in neurons (11). Recently, we found that *GDAP1* deficiency induces anomalous distribution of the mitochondrial network and affects Ca^{2+} homeostasis by reducing store-operated Ca^{2+} entry (SOCE) (12).

To identify genetic modifiers of clinical expression variability, different strategies can be used, i.e. functional and/or positional candidate genes. The *junctophilin-1* (*JPH1*) gene is close to the *GDAP1* gene at 8q21.1 (chromosome 8: 75,146,935–75,233,563; reverse strand). Four *junctophilin* genes (*JPH1-4*) are known in vertebrates and encode for a family of junctional membrane complex (JMC) proteins, which are highly conserved in evolution (13). The JPH proteins contribute to the formation of JMCs in excitable cells by anchoring the endoplasmic reticulum (ER) to the plasma membrane (PM) or the sarcoplasmic reticulum (SR) to T-tubules in muscle cells, where these structures play a role in controlling intracellular Ca^{2+} homeostasis (13–17). JPH1 and JPH2 are expressed in skeletal muscle (13,15), and their suppression leads to SOCE activity disruption (17,18).

To explore the possibility that *JPH1* nucleotide variants may modify the disease phenotype in individuals with CMT2K, we performed a mutational screening in the *JPH1* gene in 24 carriers of the *GDAP1* p.R120W mutation. The characterization of the *JPH1* p.R213P mutation in one patient with a more severe clinical picture led us to thoroughly investigate the relation between JPH1 and GDAP1. These two proteins play a role in Ca^{2+} homeostasis, and in the present report, we demonstrate that JPH1, but not the p.R213P mutant, is able to rescue the SOCE defects in *GDAP1*-silenced cells. The combination of both mutated proteins dramatically reduces SOCE activity, resembling the effect observed in *GDAP1* knock-down (KD) cells. Hence, the *JPH1* p.R213P seems to act as a negative modifier of the *GDAP1* p.R120W mutation. On the basis of these findings, we conclude that JPH1 and GDAP1 share a common pathway in which JPH1 can act as a modifier of disease severity in patients affected by a *GDAP1*-related CMT neuropathy.

RESULTS

JPH1-GDAP1 cluster forms a paralogon and is conserved in vertebrates

The comparison of vertebrate *GDAP1* orthologous regions (Fig. 1A) showed that the organization of the *JPH1-GDAP1* cluster is highly conserved. *JPH1* and *GDAP1* genes are close and are disposed in opposite orientations, and this genomic relation is conserved among vertebrate genomes. Moreover, the same scenario is observed when comparing the paralogous *GDAP1L1* (*ganglioside-induced differentiation-associated protein 1-like 1*) locus, which is near the *JPH2* gene (Fig. 1B). The *JPH2-GDAP1L1* syntenic cluster is also conserved among vertebrate genomes. These data allow us to conclude that the duplication of *GDAP1-GDAP1L1* is linked to the *JPH1-JPH2* duplication and both gene clusters constitute a highly conserved paralogon in vertebrates.

Bacterial genes with a related function are organized into operons. Blocks of genes that participate in the same process have also been described in eukaryotic genomes (19–22). Thus, JPH1 and GDAP1 have a role in the Ca^{2+} homeostasis, and in fact, lacking GDAP1 and JPH1 lead to abnormal SOCE processes (12,17). Taken as a whole, all these findings indicate that JPH1 is a good positional and functional candidate to modify GDAP1 function.

JPH1 is expressed in both skeletal muscle and neuronal tissues

GDAP1 is primarily expressed in neurons (9), whereas *JPH1* is predominantly expressed in skeletal muscle (13). We analysed *Jph1* mRNA and protein in neuronal and muscle tissues of adult mice to get more insight into its expression in the peripheral nervous system, and we analysed the expression in primary cultures of motor neuron and Schwann cell lines. We observed that *Jph1* is expressed in all the investigated tissues and in both cell types (Fig. 1C). The western blot (WB) analysis indicated that the Jph1 protein is abundantly expressed in skeletal muscle, consistent with previous reports, and neuronal tissues (Fig. 1D). Thus, *Jph1* is also expressed in the central and peripheral nervous systems, similar to *Gdap1*, suggesting that both proteins are present in the same neural tissues, and therefore, alterations in both genes can modify Ca^{2+} homeostasis in the same cell types and may contribute to the pathogenesis of this disease.

To validate the previous findings, we analysed the presence of JPH1 in cell lines derived from human tissues by WB. We selected SH-SY5Y, which is a tumour cell line that originated from neural crest cells; HeLa, which is a human epithelial carcinoma cell line; human fibroblasts; and rhabdomyosarcoma, which is a human skeletal muscle sarcoma-derived cell line. We detected protein in rhabdomyosarcoma, SH-SY5Y and HeLa (Fig. 1E). Therefore, SH-SY5Y cells are an excellent model for investigating the relation between these proteins because *JPH1* and *GDAP1* are expressed in this cell line (9–11).

JPH1 variants in *GDAP1* p.R120W-affected carriers

The mutation analysis of 24 carriers revealed two different mutations in the *JPH1* gene: c.638G>C (p.R213P) in one patient from family fCMT-408 (Fig. 2A) and c.1870G>C (p.D624H) in one patient from family fCMT-213 and in three affected siblings from family fCMT-214 (Supplementary Material, Fig. S1). Both nucleotide variants are annotated as single nucleotide polymorphisms (SNPs) in the public databases (UCSC Genome Browser, http://genome.ucsc.edu/; Ensembl, http://www.ensembl.org/index.html; NCBI, http://www.ncbi.nlm.nih.gov/). The c.638G>C alteration (rs201314759; minor allele frequency, MAF, [G] < 0.01) is predicted as a damaging mutation by both SIFT and PolyPhen-2 algorithms. No homozygous individuals for the uncommon allele are annotated in the consulted databases. The c.1870G>C variant (rs16938828; MAF [G] = 0.01) is predicted as a tolerated mutation by both computational tools. Only one individual from the European–American population who is homozygous for the allele with minor frequency is annotated.

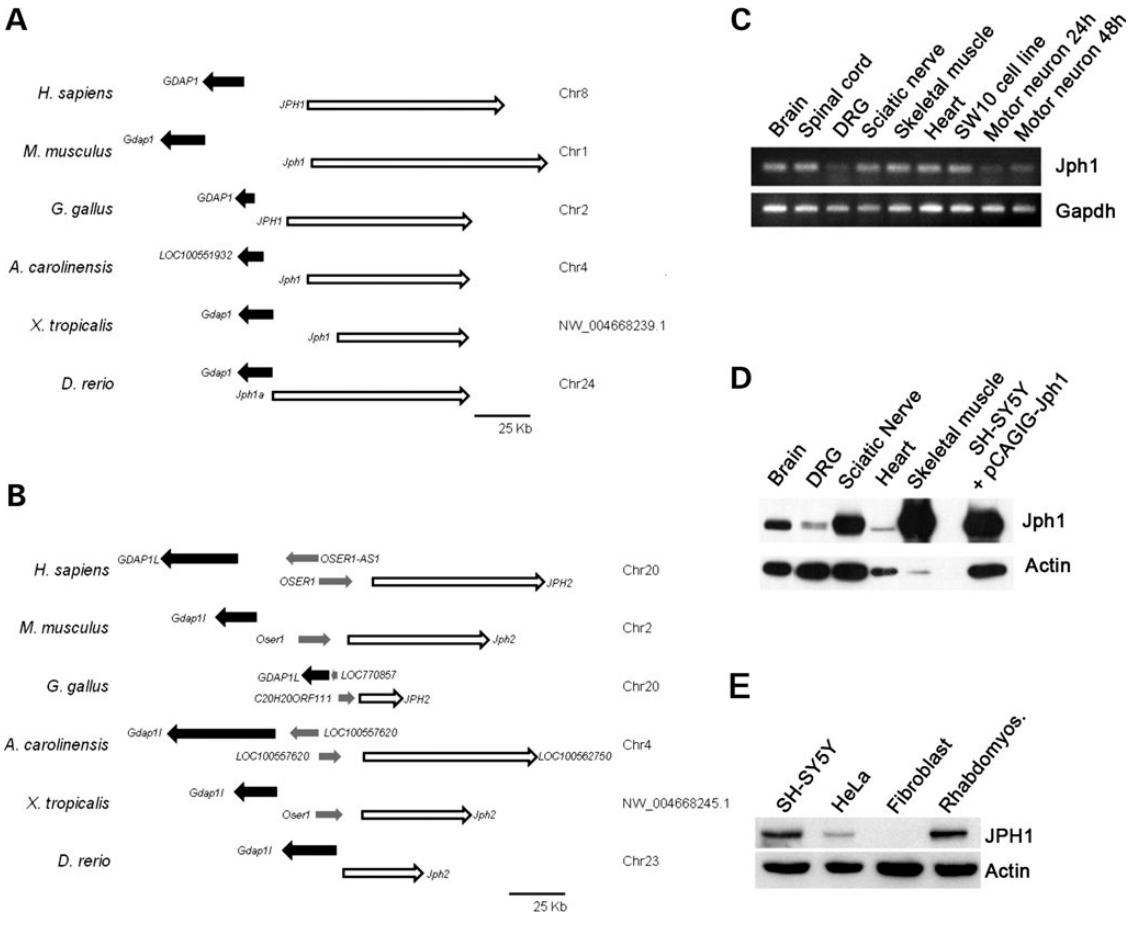

Figure 1. JPH1 and GDAP1 form a conserved paralogon, and their expression coincides in the nervous system. (**A**) Comparative genomics at the *GDAP1* and (**B**) *GDAP1L1 loci* in vertebrates. Orthologues of *GDAP1* or *GDAP1L1* are represented by black arrows, whereas orthologues of *JPH1* or *JPH2* are represented by white arrows. Grey arrows represent other predicted genes. The organism names and chromosome/scaffold numbers are also shown. Scale bar represents 25 kb. (**C**) RT-polymerase chain reaction (PCR) analyses of *Jph1* mRNA expression in adult mice tissues. *Jph1* expression was also evaluated in Schwann cell and motor neuron cell cultures. *Gapdh* expression was included as a control for amplification. (**D**) WB analyses of the Jph1 protein in adult mice tissues and (**E**) in human-derived cell lines. Murine Jph1 overexpression in SH-SY5Y cells was used as the positive control. Actin was used as the loading control.

All JPH proteins contain eight membrane occupation and recognition nexus (MORN) motifs clustered near the amino terminus, followed by an α-helix domain and a carboxyl-terminus transmembrane region (23,24). The p.R213P variant is placed in the joining region, which is between the first six and the last two MORN motifs, and might serve an accessory protein-binding region; the p.D624H variant is close to the membrane-spanning segment (Fig. 2B). These alterations may affect the interaction with the PM or ER and, therefore, may prevent JMC stabilization.

The *JPH1* p.R213P and *GDAP1* p.R120W double carrier shows a more severe clinical picture

Clinical pictures of families fCMT-213 and fCMT-214 were thoroughly described by Sivera *et al*. (6) and correspond to families A and C, respectively, in that paper (Supplementary Material, Fig. S1). Patients belonging to these two families show an axonal neuropathy presenting a mild-to-moderate phenotype (Charcot–Marie–Tooth neuropathy score, CMTNS, ranges from 5 to 21).

Clinical and electrophysiological data corresponding to family fCMT-408 are shown in Tables 1 and 2, respectively. The proband (Fig. 2A, ID no. III:1) is affected by a moderate motor and sensory neuropathy (CMTNS2 score of 9; 29 years old; Table 1) with amyotrophy present in the posterior compartments of the legs and sole muscles, and high-arched feet and claw toes. Nerve conduction studies showed absent sensory nerve action potentials (SNAP) on all the examined nerves and decreased compound muscle action potentials (CMAPs) on posterior tibial nerves. Her parents noticed that she was clumsy in sports before the age of 10; however, she was otherwise normal. At the age of 15, she was unsteady when walking with high heel shoes and she was aware that her feet were highly arched. The proband's father (Fig. 2A, ID no. II:4) and two carrier uncles (Fig. 2A, ID no. II-1 and II-2) showed a very mild phenotype with low CMTNS2 scores (Table 1).

Proband's muscle magnetic resonance imaging (MRI) of the lower limbs showed high signal intensity on T1-weighted images on gastrocnemius and soleus muscles, corresponding with fatty substitution (Fig. 2C). In contrast, no changes were observed in any affected relatives.

Sural nerve biopsy was performed on the proband and disclosed endoneural fibrosis and a severe reduction of myelinated

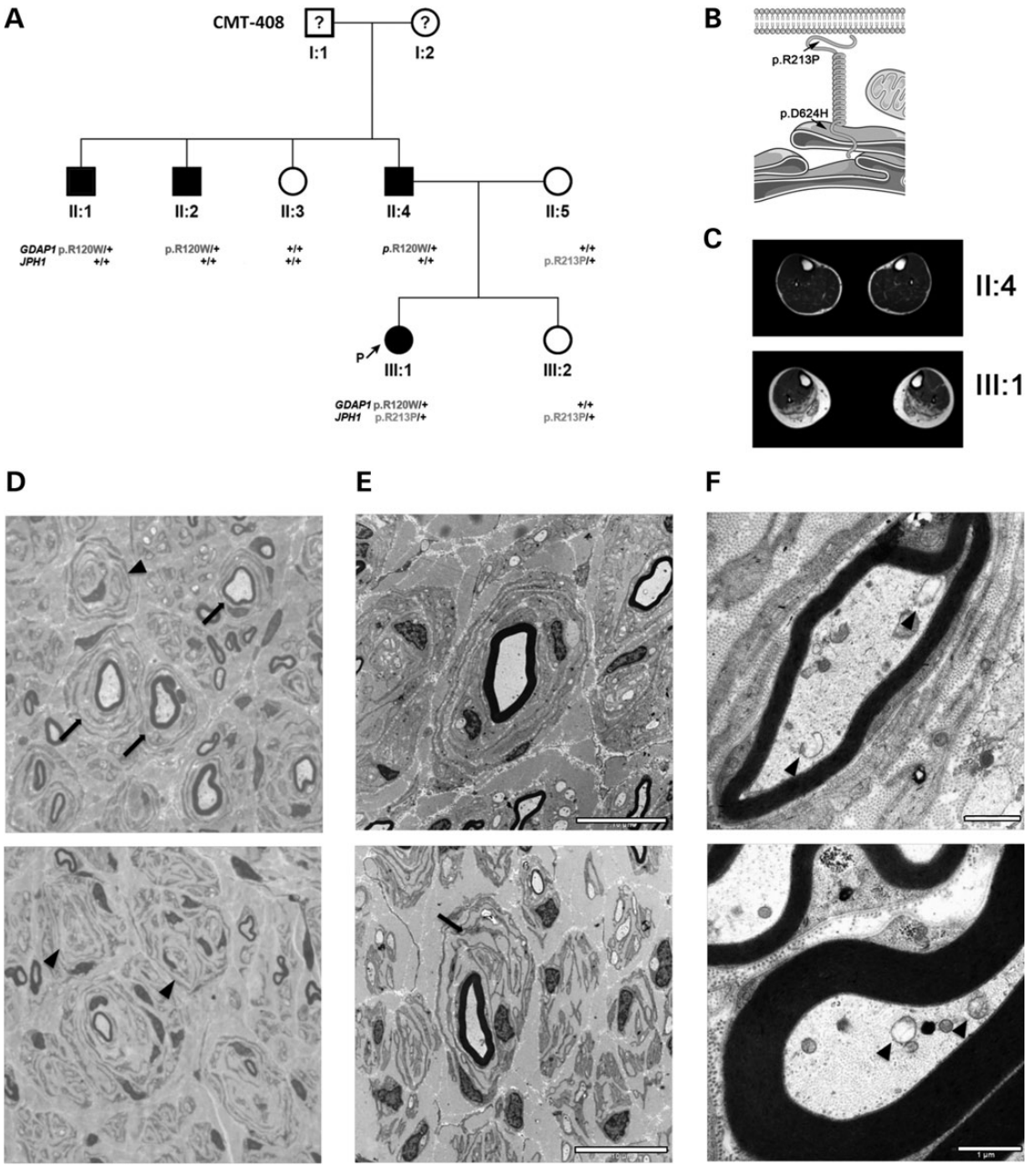

Figure 2. More severe clinical picture in the *JPH1*$^{p.R213P}$ and *GDAP1*$^{p.R120W}$ double carrier. (**A**) Pedigree of the fCMT-408 family. All the affected individuals harbour the *GDAP1* p.R120W mutation, whereas the proband carries both *GDAP1* p.R120W and *JPH1* p.R213P mutations. (**B**) Schematic representation of the JPH1 protein; locations of the JPH1$^{p.R213P}$ and JPH1$^{p.D624H}$ variants are indicated with arrows. This figure was produced using ServierMedical Art (http://www.servier.com/serviermedical-art/powerpoint-image-bank). (**C**) Muscle MRI of the calf muscles of the II:4 and III:1 patients, showing fatty substitution only in the proband. (**D**–**F**) Neuropathological findings of the sural nerve biopsy of the proband. (D) Semi-thin transverse sections stained with toluidine blue showing a severe reduction of myelinated fibres, inappropriately thinly large myelinated fibres, numerous classic OB formations (arrows) and several large atypical OBs (arrowheads) without axons (× 100). (**E** and **F**) Electron microscopy: (E upper) classic OB with multiple layers of concentric Schwann cell cytoplasmic processes surrounding a normal myelinated axon. (E lower) Atypical OB with inner irregular interdigitating and branching Schwann cell processes (arrow). Scale bar represents 10 μm. (**F**) Myelinated axons with focal aggregates of abnormal irregular mitochondria showing swelling, vacuolar degeneration and crest disruption (arrowhead). Scale bar represents 1 μm.

fibres, particularly those fibres with large diameters, with a fibre density of 3559/mm^2 (reference values, 8000–13 000/mm^2) (Fig. 2D). Unexpected neuropathological features of hypertrophic whorls and onion bulb (OB) formations were prominent and discernible in all the fascicles. The morphological appearance of these OB formations included the following: typical OB formations, with concentrically arranged Schwann cell processes around a normal or thinly myelinated fibre, extremely large atypical OB formations and 'burnt-out' OB formations without central axons (Fig. 2D and E). Some of these large atypical OB formations had no central myelinated fibres and showed inner Schwann cell processes with an irregular branching shape

Table 1. Clinical data for the fCMT-408 family

Patient	Onset/age at exam (years)	CMTNS2	Ankle DF	Ankle PF	Toe flexion	Heel/ toe walk	Kneejerk	Anklejerk	Foot deformity	Pinprick sensory loss	Vibration sensory loss	Propioceptive sensory loss
II:1	−/53	2	5	5	5	N/N	++	++	No	N	N	N
II:2	45/52	1	5	5	5	N/N	++	++	High arches, claw toes	N	N	N
II:3	−/49	0	5	5	5	N/N	++	++	No	N	N	N
II:4	−/56	3	5	5	5	N/N	++	+	Claw toes	Ankle	Ankle	N
II:5	−/54	0	5	5	5	N/N	++	++	No	N	N	N
III:1	15/29	9	5	4	4	N/I	−	−	High arches, claw toes	Distal legs	Ankle	Ankle
III:2	−/25	0	5	5	5	N/N	++	++	No	N	N	N

CMTNS2, Charcot–Marie–Tooth neuropathy score 2; DF, dorsal flexion; I, impossible; N, normal, PF, plantar flexion.

instead of a typical concentric arrangement (Fig. 2E). Small pseudo-OBs with only one or two layers of Schwann cell processes surrounding a single axon or regenerative clusters were also recognized; however, no basal lamina or perineural cell pseudo-OBs were observed. Despite this predominantly hypertrophic pattern, regenerative clusters of small axons were also identified in several fascicles. Signs of acute axonal degeneration were absent. The electron microscopy analysis indicated that myelin compaction was normal, and no folding or thickening in the myelin sheaths was observed. In some axons, clusters of abnormal swollen mitochondria with no discernible crests and focal microtubule rarefaction were also evident (Fig. 2F).

In short, the proband presents with a moderate clinical picture that is very different compared with the phenotype described in her relatives who are carriers of the *GDAP1* p.R120W and are almost asymptomatic. In addition, relatives who only harbour the *JPH1* p.R213P mutation do not present any neurological symptoms; therefore, *JPH1* p.R213P is not sufficient to cause neurological symptoms.

JPH1 restores the *GDAP1* deficiency in KD cells

GDAP1 depletion in SH-SY5Y cells results in a significant decrease in SOCE activity and thapsigargin (TG)-induced Ca^{2+} release. This defect is associated with improper distribution of mitochondria producing Ca^{2+} inactivation of store-operated Ca^{2+} (SOC) channels due to Ca^{2+} buffering failures (12). In addition, reduced JPH1 protein levels are also related to a defective SOCE caused by failures in SOC channel formation in junction membrane structures (17,18). To investigate whether JPH1 and GDAP1 play a role in the same process, we overexpressed JPH1 in the control SH-SY5Y cell line and in the *GDAP1*-silenced SH-SY5Y cell line (Supplementary Material, Fig. S2A). We showed that the expression of JPH1 and JPH1$^{p.D624H}$ in control cells does not alter resting Ca^{2+}, whereas the expression of JPH1$^{p.R213P}$ decreases basal cytosolic Ca^{2+} (Fig. 3A). Because of this finding, all values were normalized to the basal ratio to compare the response of the investigated JPH1 forms. The overexpression of wild-type (WT) or mutated JPH1 does not produce significant alterations in control cells, either in TG-induced Ca^{2+} release or in SOCE amplitude (Fig. 3B), suggesting that these missense variants themselves do not cause physiological alterations. Surprisingly, when we express JPH1 in *GDAP1*-silenced cells, SOCE activity is restored and increases the TG-induced Ca^{2+} release and the SOCE amplitude (Fig. 3C), as observed by GDAP1 overexpression. In contrast, JPH1$^{p.R213P}$ cannot restore the SOCE activity, whereas JPH1$^{p.D624H}$ has an effect similar to JPH1 (Fig. 3C). In summary, JPH1 is able to restore SOCE activity in the absence of GDAP1, suggesting that the function of both proteins is closely related. Nevertheless, JPH1$^{p.R213P}$ alone cannot restore SOCE activity; therefore, JPH1$^{p.R213P}$ seems to require GDAP1 to correctly function.

To investigate the effect of reduced SOCE activity in *GDAP1* KD cells expressing JPH1 constructs, we used ionomycin, which is a Ca^{2+} ionophore that depletes the ER-Ca^{2+} stores by either directly transporting ions or functioning as an ion channel, producing total discharge of Ca^{2+} from the ER and other minor stores. As shown in Figure 3D, chronic silencing of *GDAP1* produces a significant reduction in the cell's total Ca^{2+} content compared with SH-SY5Y control cells. JPH1 and JPH1$^{p.D624H}$ expression restores the Ca^{2+} content at the control cell level. This effect is consistent with the previously described role of JPHs in controlling Ca^{2+} homeostasis (17). In contrast, neither JPH1$^{p.R213P}$ nor GDAP1 expression can restore the Ca^{2+} content, suggesting that both proteins have a close function but not in the same process.

GDAP1 depletion affects proper mitochondrial network distribution and leads to impairment of the SOCE process in SH-SY5Y cells (12). Thus, to explore whether the rescue of SOCE by JPH1 is dependent of mitochondria, we measured SOCE activity after JPH1 overexpression in the presence of the mitochondrial function blockers antimycin A/oligomycin. As shown in Figure 3E, the presence of mitochondrial blockers produced severe inactivation of SOCE in control cells. Surprisingly, SOCE activity in JPH1-overexpressing cells was no longer inhibited by mitochondrial blockers, indicating that the restoration of SOCE activity by JPH1 in *GDAP1* deficient cells is not related to the recovery of mitochondrial distribution/function. In summary, we confirmed that JPH1 recovers SOCE activity in cells lacking *GDAP1* by a non-mitochondrial mechanism.

JPH1 is in both ER and mitochondrial-associated membranes

Because we have previously observed that JPH1$^{p.R213P}$ cannot restore the SOCE response in the absence of GDAP1 (Fig. 3C), we investigated the relation between JPH1 and mitochondria

Table 2. Nerve conduction data for the fCMT-408 family

Patient	Median nerve		Peroneal nerve		Post tibial nerve		Radial nerve		Median nerve		Sural nerve		Superficial peroneal nerve	
	CMAP (mV)	MNCV (m/s)	CMAP (mV)	MNCV (m/s)	CMAP (mV)	MNCV (m/s)	SNAP (μV)	SNCV (m/s)	SNAP (μV)	SNCV (m/s)	SNAP (μV)	SNCV (m/s)	SNAP (μV)	SNCV (m/s)
II:1	10.1	57.9	12.6	47.1	14.4	46.0	6.5	57.1	ND	ND	3.8	51.0	2.1	47.4
II:2	15.0	52.7	10.9	38.8	13.1	39.2	12.3	51.2	ND	ND	3.9	40.3	2.5	38.5
II:4	6.0	54.5	8.5	40.0	9.2	40.6	6.9	47.8	9.2	50.0	NR	NR	NR	NR
II:5	13.4	53.5	12.3	45.7	15.8	43.4	13.6	50.2	17.2	54.6	14.5	53.7	ND	ND
III:1	9.4	54.1	9.0	43.2	2.6	39.2	NR	NR	NR	NR	NR	NR	NR	NR
III:2	13.7	55.7	11.4	46.3	16.3	40.2	14.5	52.2	18.3	56.3	13.7	52.2	ND	ND

CMAP, compound muscle action potential; MNCV, motor nerve conduction velocity; ND, not done; NR, no response; SNAP, sensory nerve action potential; SNCV, sensory nerve conduction velocity.

and the exact cellular location of JPH1. We overexpress JPH1::GFP in SH-SY5Y control cells (Supplementary Material, Fig. S2B) and, along with some patches in lysosomes (LAMP1) and in the Golgi apparatus (β-COP), we observed that JPH1 primarily colocalizes with the ER marker GRP94 (Fig. 4A). Moreover, JPH1 partially colocalizes with mitochondria, likely corresponding to mitochondria-associated membrane (MAM) contact points (Fig. 4A). The same localization in the ER can be observed when the experiment is performed with JPH1$^{p.R213P}$ and JPH1$^{p.D624H}$ (Fig. 4B); therefore, neither of these mutations alters the proper localization of the mutant proteins.

Because GDAP1 has been previously described as a protein placed at MAMs (12) and JPH1 colocalizes in some patches with mitochondria, next, we searched for the specific locations of JPH1 and GDAP1 in specific organelles and membranes. Differential centrifugation was performed to separately obtain ER, crude mitochondria, pure mitochondria and MAMs. Shared localization of JPH1 and GDAP1 in the MAMs compartment (Fig. 4C) suggests that both proteins may play a role in mitochondria–ER function.

JPH1 colocalizes with STIM1 during ER-Ca^{2+} release

ER-Ca^{2+} store depletion activates SOCE through a distinctive rearrangement of STIM1 and Orai1; STIM1 oligomerizes and migrates to the ER–PM junctions (25), and Orai1 is accumulated at PM sites directly opposite STIM1 (26,27). During ER-Ca^{2+} release, mitochondria alter their morphology and relocate near subplasmalemmal sites, where mitochondria play a key role in maintaining sustained SOCE and adequate ER refilling by regulating Ca^{2+} fluxes within the cell (28). We performed colocalization experiments with the JPH1-CFP construct expressed in SH-SY5Y cells using the markers STIM1-YFP and Cyt *c*. Under resting conditions, we observed that all forms of JPH1 colocalize with STIM1. All these proteins present a reticular and diffuse expression pattern corresponding to an ER pattern (Supplementary Material, Fig. S3A). After TG induction, STIM1 forms puncta and colocalizes with Orai1 (Supplementary Material, Fig. S3B), and JPH1 also forms puncta and colocalizes with STIM1 (Fig. 4D). Both JPH1$^{p.R213P}$ and JPH1$^{p.D624H}$ do not greatly alter this pattern. To better understand the relation among these three components of the SOCE mechanism, we quantified the colocalization between JPH1 and STIM1 and between JPH1 and mitochondria using the Manders' colocalization index. As shown in Figure 4E, no difference is observed in the colocalization between the JPH1 constructs and STIM1 after TG induction. The decrease in JPH1 and STIM1 colocalization between both conditions can be the consequence of STIM1 migration and oligomerization to ER–PM puncta. This effect was also observed for the two mutant proteins. In contrast, TG-induced Ca^{2+} depletion significantly reduces the colocalization between either JPH1 or JPH1$^{p.D624H}$ and mitochondria (Fig. 4F). However, this decrease is less obvious for JPH1$^{p.R213P}$, likely due to difficulties in the oligomerization (Fig. 4D, middle panel).

Colocalization of JPH1$^{p.R213P}$ with STIM1 during ER-Ca^{2+} release is dependent on GDAP1

Previous results have demonstrated that JPH1$^{p.R213P}$ overexpression cannot restore SOCE activity in *GDAP1*-silenced cells

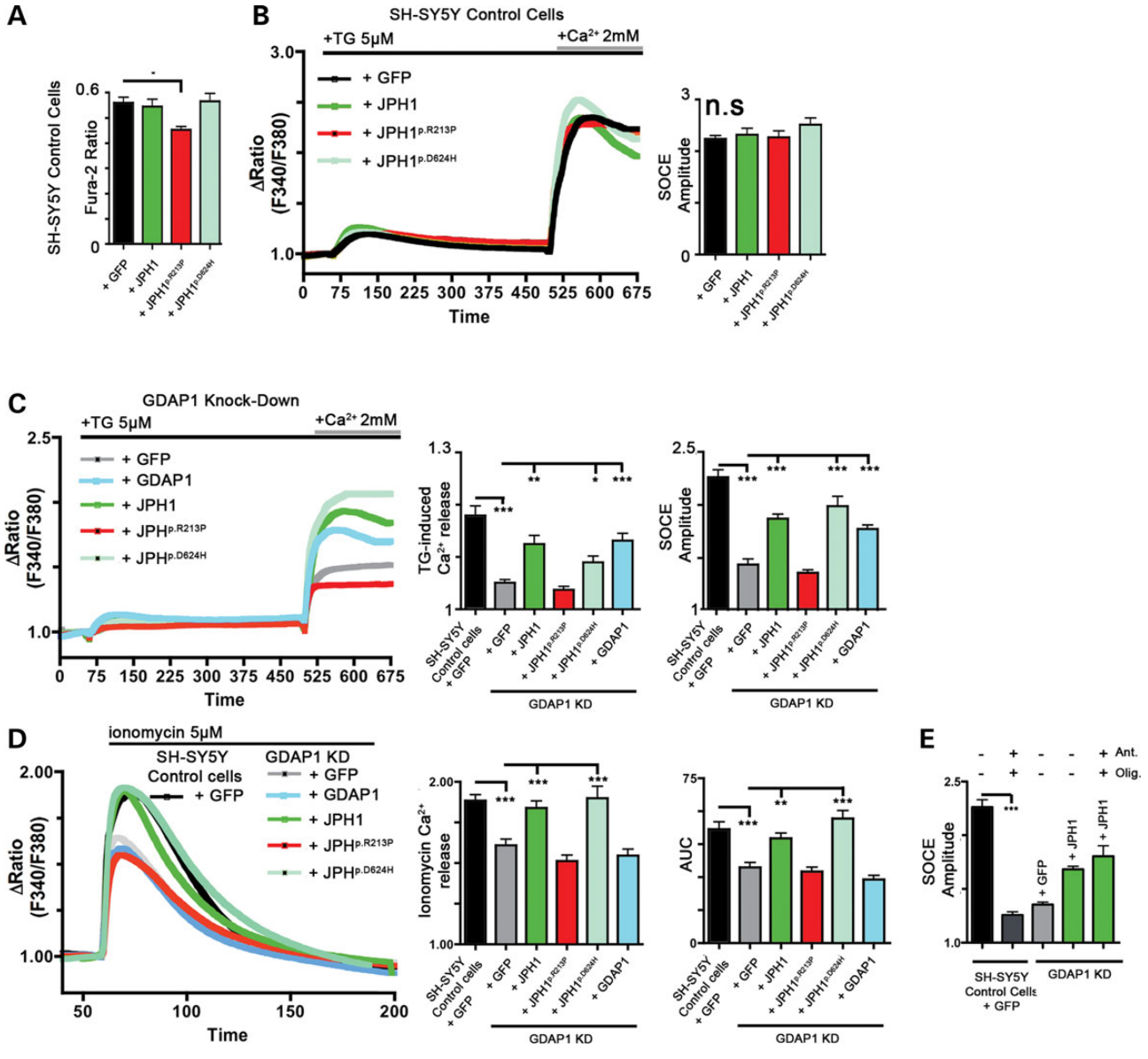

Figure 3. JPH1 recovers the SOCE deficiency of the *GDAP1* KD cell line, whereas the JPH1^{pR213P} mutation fails to rescue this deficiency. (**A**) Analysis of basal cytosolic Ca^{2+} measured in SH-SY5Y control cell line loaded with Fura-2 and expressing pCAGIG bicistronic plasmid overexpressing JPH1, JPH1$^{p.D624H}$ and JPH1$^{p.R213P}$. (**B**) Normalized Fura-2 traces in the SH-SY5Y control cell line and (**C**) in the GDAP1 KD cells. ER-Ca^{2+} release was induced by adding 5 μM TG before addition of 2 mM $CaCl_2$ to induce SOCE. To evaluate the effect of JPH1 and mutated forms, the TG-induced Ca^{2+} release and SOCE amplitude were quantified. (**D**) Comparison of ER-Ca^{2+} content by measuring ionomycin-induced Ca^{2+} release in the SH-SY5Y cell line or in the GDAP1 KD cell line overexpressing the indicated plasmids. Total discharge of Ca^{2+} from the ER and from other minor stores was induced by adding 5 μM ionomycin. The effect of JPH1 and mutated forms was evaluated by quantifying the ionomycin-induced Ca^{2+} release and the area under the curve. (**E**) SOCE analysis, measured by comparing SOCE amplitudes, in the SH-SY5Y control cell line or in the *GDAP1* KD cells overexpressing JPH1 in the presence of the mitochondrial function blockers antimycin A (5 μg/ml) and oligomycin (0.5 μg/ml). One-way ANOVA, Tukey's multiple comparison test: $^{*}P < 0.05$; $^{**}P < 0.01$; $^{***}P < 0.001$. Error bars represent the SEM.

(Fig. 3C) and that JPH1 colocalizes with STIM1 (Fig. 4D), suggesting a role for JPH1 in ER–PM sites. To explore whether the JPH1 function is modified by GDAP1, we performed identical studies in *GDAP1*-silenced cells. First, we confirmed that the colocalization of STIM1 and Orai1 is also present in *GDAP1* KD cells and that STIM1 forms puncta after TG-induced Ca^{2+} release (Supplementary Material, Fig. S4A), which is consistent with a previous report demonstrating that reduced SOCE in *GDAP1* KD cells is associated with a mitochondrial defect (12). JPH1 colocalizes with STIM1 in *GDAP1*-depleted resting cells (data not shown), as observed in SH-SY5Y cells (Supplementary Material, Fig. S3A). ER-Ca^{2+} release after TG treatment in *GDAP1* KD cells enhance oligomerization of STIM1, JPH1 (Fig. 5A) and JPH1$^{p.D624H}$ (Fig. 5B). Surprisingly, JPH1$^{p.R213P}$ expression in *GDAP1*-depleted cells shows defects in STIM1 oligomerization and prevents JPH1 migration with STIM1 (Fig. 5C). As expected, this defect is rescued when GDAP1 is expressed (Fig. 5D). These observations are supported by the quantification results of the colocalization of JPH1 and JPH1 mutant forms with STIM1 (Fig. 5E). Only JPH1$^{p.R213P}$ presents a significant decrease in

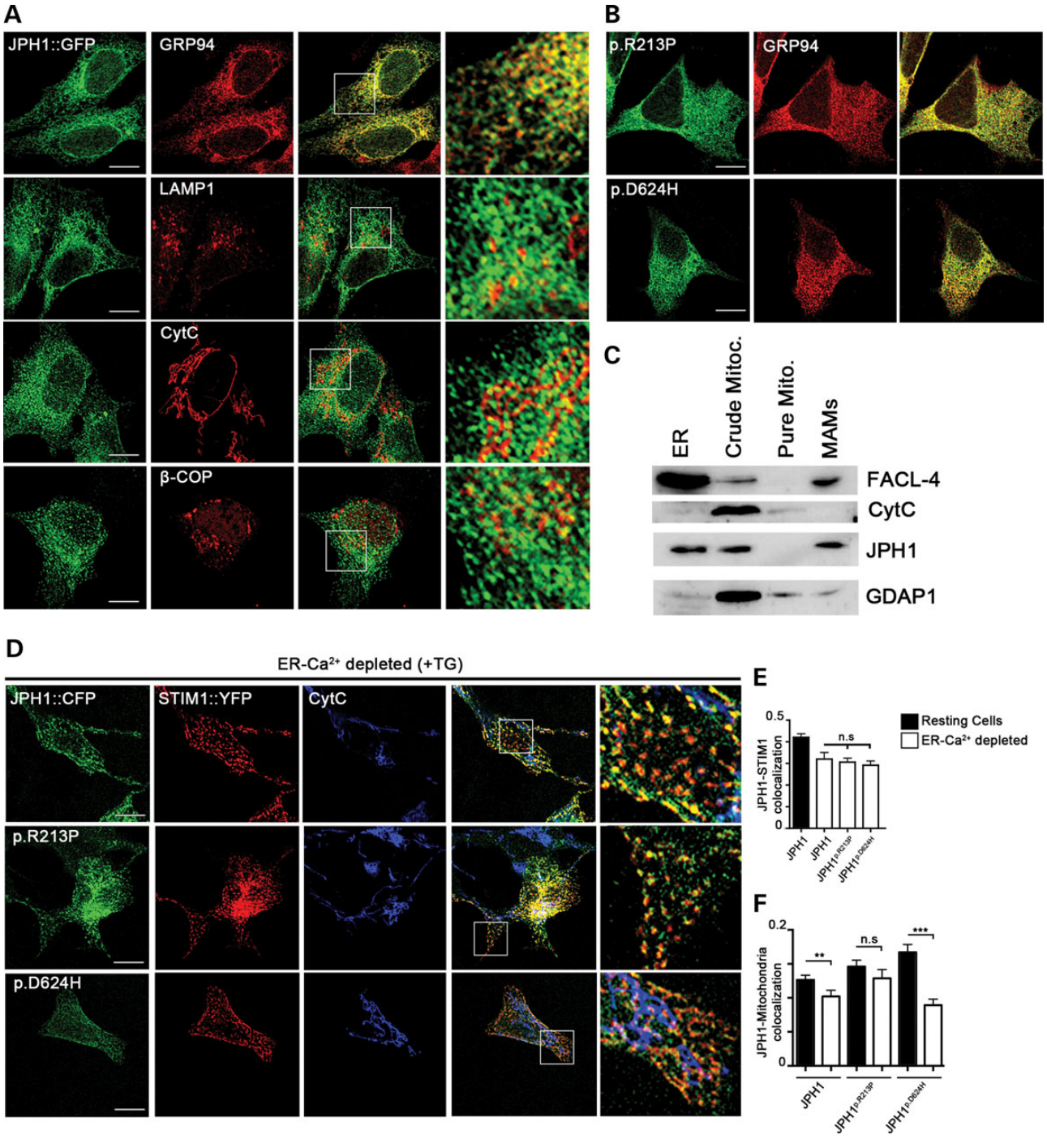

Figure 4. JPH1 is in the ER and MAMs and colocalizes with STIM1 during ER-Ca^{2+} release. (**A**) Immunofluorescence of the SH-SY5Y cell line overexpressing GFP-tagged WT JPH1 and (**B**) $JPH1^{p.R213P}$ or $JPH1^{p.D624H}$ to study the subcellular distribution of JPH1 forms. GRP94 was used as an ER marker, LAMP1 as a lysosomal marker, Cyt *c* as a mitochondrial marker and β-COP as a Golgi marker. GFP-tagged proteins are represented with green signals, whereas the subcellular markers are represented with red signals. An enlargement of the boxed region in the merge images is also shown. Scale bar represents 10 μm. (**C**) WB of MAMs obtained from mouse brains, showing the presence of Jph1 in the MAM fraction. FACL-4 was used as the MAM marker. (**D**) Immunofluorescence of the SH-SY5Y control cell line overexpressing CFP-tagged WT or mutated JPH1 (green signal) and STIM1-YFP (red signal) after ER-Ca^{2+} release. Cyt *c* was used as a mitochondrial marker (blue signal). ER-Ca^{2+} release was induced by adding 5 μM TG in 30 mM D-glucose Ca^{2+}-free HEPES-buffered controlled salt solution (HCSS) buffer for 10 min before fixation. An enlargement of the boxed region in the merge images is also shown. Scale bar represents 10 μm. **(E** and **F)** Quantification of the colocalization measured by Manders' coefficient. **(**E) Colocalization between JPH1 versus STIM1 and (F) JPH1 versus mitochondria under resting conditions (black bars) or TG-induced conditions (white bars). One-way ANOVA, Tukey's multiple comparison test: $^{*}P < 0.05$; $^{**}P < 0.01$; $^{***}P < 0.001$. Error bars represent the SEM.

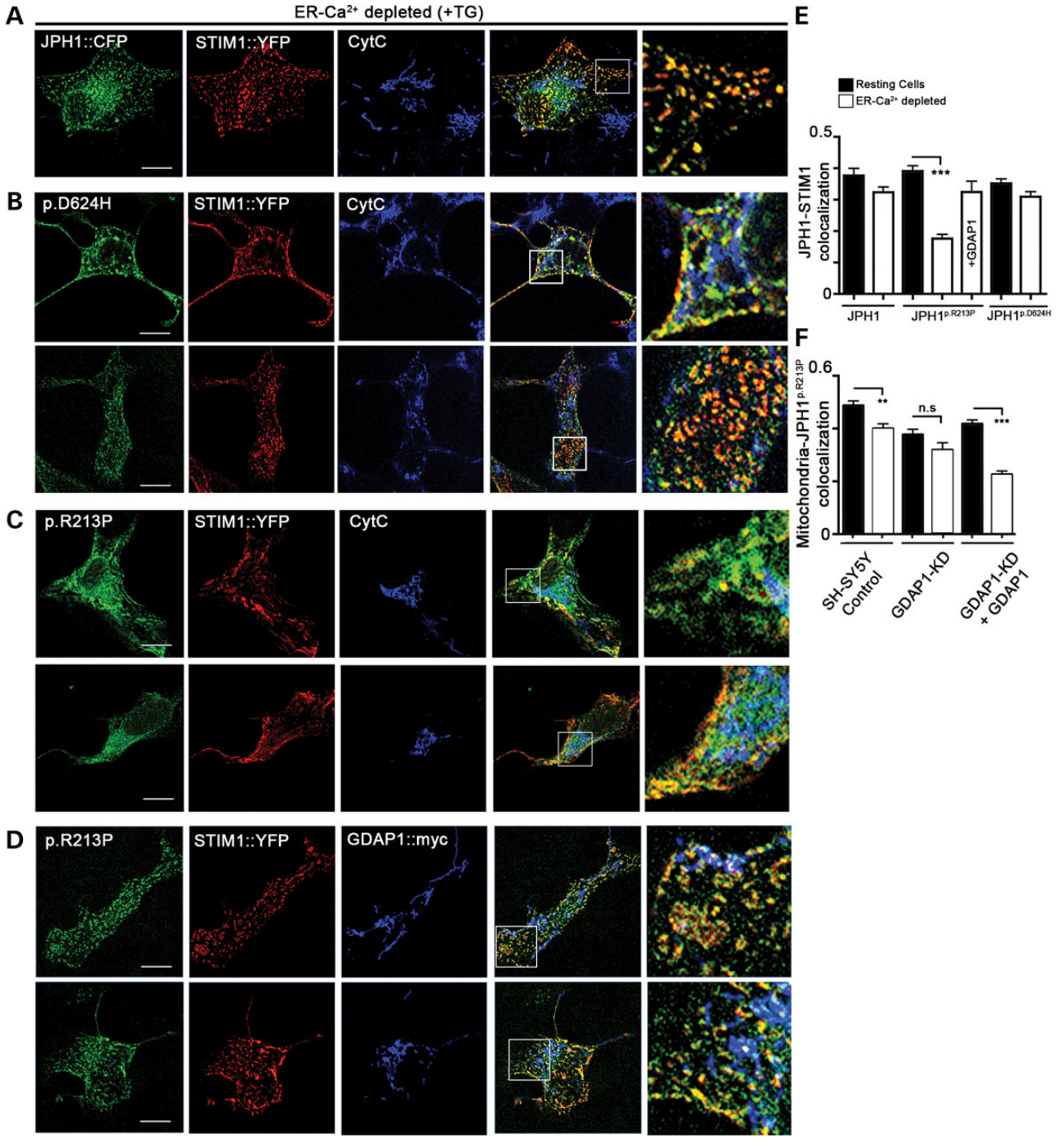

Figure 5. Oligomerization of JPH1$^{p.R213P}$ during ER-Ca^{2+} release is dependent on GDAP1. (**A**) Immunofluorescence of *GDAP1* KD cells overexpressing STIM1-YFP (red signal) and CFP-tagged WT JPH1, (**B**) JPH1$^{p.D624H}$ or (**C**) JPH1$^{p.R213P}$ forms (green signal) after TG-induced Ca^{2+} release. Cyt *c* was used as a mitochondrial marker (blue signal). (**D**) Immunofluorescence of *GDAP1* KD cells overexpressing CFP-tagged JPH1^{R213P} (green signal), STIM1-YFP (red signal) and GDAP1-myc (blue signal) during TG-induced Ca^{2+} release. ER-Ca^{2+} release was induced by adding 5 μM TG in 30 mM D-glucose Ca^{2+}-free HCSS buffer for 10 min before fixation. For the B, C and D, two different representative images are shown. An enlargement of the boxed region in the merge images is also shown. Scale bar represents 10 μm. **(E)** Quantification of the colocalization measured by Manders' coefficient between the different forms of JPH1 and STIM1 in *GDAP1* KD cells under resting (black bar) or TG-induced conditions (white bar). Colocalization between JPH1$^{p.R213P}$ and STIM1::YFP was recovered after overexpression of GDAP1::myc. **(F)** Colocalization between mitochondria and JPH1$^{p.R213P}$ in SH-SY5Y cells, in *GDAP1* KD cells and in *GDAP1* KD cells overexpressing GDAP1. *T*-tests were used to compare between pairs in resting and induced conditions: $^{*}P < 0.05$; $^{**}P < 0.01$; $^{***}P < 0.001$. Error bars represent the SEM.

the colocalization with STIM1 compared with JPH1, which is evidently restored in the presence of GDAP1. In addition, the limited response of JPH1$^{p.R213P}$ after TG-induction is also evident in the colocalization with the ER, supporting a defect in JPH1$^{p.R213P}$ migration in *GDAP1* KD cells (Supplementary Material, Fig. S4B). The different colocalization pattern of

JPH1$^{p.R213P}$ with STIM1 could explain why the overexpression of JPH1$^{p.R213P}$ in *GDAP1* KD cells does not recover SOCE activity as JPH1 and JPH1$^{p.D624H}$ do. To confirm this JPH1 migration defect, we analysed the colocalization of mitochondria and JPH1. As shown in Supplementary Material, Figure S5A, after ER-Ca^{2+} depletion, JPH1 decreases colocalization with mitochondria in control cells due to its capacity to relocate with STIM1 in PM sites, but in contrast, in *GDAP1* KD cells, we cannot observe changes in the level of colocalization of JPH1$^{p.R213P}$ (Fig. 5F). GDAP1 expression recovers the observed shift between JPH1 and mitochondria in SH-SY5Y cells. Thus, in the absence of GDAP1, JPH1$^{p.R213P}$ loses the proper localization, and the JPH1-STIM1 colocalization in ER–PM puncta structures is recovered when GDAP1 is present. To determine whether this recovery is due to a physical interaction between both proteins, we performed coimmunoprecipitation (CoIP) assays of the WT and mutated JPH1 forms and GDAP1 in basal and TG-induced conditions. The results were negative in all the cases (Supplementary Material, Fig. S5B). The exact mechanism by which JPH1 localization is modified by GDAP1 remains elusive.

GDAP1$^{p.R120W}$ retains JPH1 in mitochondria

Previous findings revealed that JPH1-STIM1 colocalization in ER–PM puncta structures is GDAP1-dependent. To determine how GDAP1$^{p.R120W}$ could affect protein localization, we performed colocalization studies of the JPH1-CFP construct expressed in *GDAP1* KD cells with STIM1-YFP and GDAP1$^{p.R120W}$ constructs in resting conditions and after ER-Ca^{2+} release. The expression patterns of JPH1 and STIM1 under both conditions are quite similar for the WT and mutated forms of JPH1, although there is a fraction of JPH1 that clearly colocalizes with mitochondrial GDAP1$^{p.R120W}$, and STIM1 seems to previously be in puncta structures (Fig. 6A). The depletion of ER-Ca^{2+} contents shows the increase in STIM1 oligomerization in puncta structures, whereas JPH1 colocalizes with mitochondrial GDAP1$^{p.R120W}$ (Fig. 6B). However, JPH1 and JPH1$^{p.D624H}$ share a similar pattern. These findings are corroborated by the quantification estimated by Manders' coefficient. As shown in Figure 6D and as we previously observed in SH-SY5Y control cells (Fig. 4D and E), depletion of ER-Ca^{2+} leads to a decrease of colocalization of JPH1 and STIM1 most likely due to STIM1 migration and oligomerization to ER–PM site. When GDAP1$^{p.R120W}$ is included, the colocalization index of JPH1 and STIM1 is lower and similar for the WT and the mutated forms of JPH1 under both resting and TG-induced conditions. However, under resting conditions, STIM1 also appears in puncta structures, suggesting a defect produced by the presence of the *GDAP1* mutation. In *GDAP1* KD cells expressing GDAP1$^{p.R120W}$, the colocalization index for JPH1 and mitochondria is notably stronger for JPH1$^{p.R213P}$ compared with controls in resting conditions (Fig. 6D). After TG induction, mitochondria-JPH1 colocalization increases for the three investigated JPH1 variants: GDAP1$^{p.R120W}$ causes the three JPH1 forms to be retained in mitochondria. In control cells, JPH1 and STIM1 are placed in ER–PM puncta structures (Fig. 4D), where JPH1 would stabilize the structure to allow SOCE activity. Thus, the coexistence of GDAP1$^{p.R120W}$ and JPH1$^{p.R213P}$ would prevent the proper functioning of JPH1 because JPH1 remains retained in mitochondria. To better clarify JPH1 and GDAP1$^{p.R120W}$ expression patterns, we performed additional colocalization studies using markers for mitochondria and ER. JPH1 strongly colocalizes with the ER and mitochondria (Supplementary Material, Fig. S6). Taken together, the colocalization of GDAP1$^{p.R120W}$ with JPH1$^{p.R213P}$ is much more remarkable compared with either JPH1 or JPH1$^{p.D624H}$. Once again, the presence of JPH1 in mitochondria cannot be explained by interaction between JPH1s and GDAP1$^{p.R120W}$ (Supplementary Material, Fig. S5C).

GDAP1$^{p.R120W}$ together with JPH1$^{p.R213P}$ inhibits SOCE activity

In the presence of GDAP1, both WT and mutated JPH1 work properly (Fig. 3B). In contrast, JPH1 or GDAP1 overexpression in *GDAP1*-silenced cells restores SOCE activity; however, this restoration does not occur for JPH1$^{p.R213P}$ (Fig. 3C). Because GDAP1$^{p.R120W}$ seems to retain JPH1 in mitochondria, the next step was to clarify the effect of the combination of GDAP1$^{p.R120W}$ and JPH1 on Ca^{2+} homeostasis. Because both mutations are heterozygous in the proband, we hypothesize that the most reliable method to simulate this effect in our cell models was to use the control cell line to overexpress these protein variants. We cotransfected SH-SY5Y cells with the bicistronic plasmid pCAGIG carrying the JPH1 forms and a construct of GDAP1 and GDAP1$^{p.R120W}$ fused to mCherry in the N-terminus. The analysis of resting Ca^{2+} levels show that only the overexpression of both mutations, JPH1$^{p.R213P}$ and GDAP1$^{p.R120W}$, produces a significant increase in Fura-2 fluorescence (Fig. 7A), suggesting a previous defect in Ca^{2+} management. The analysis of SOCE dynamics showed interesting results. In Figure 7B, we confirm that the overexpression of green fluorescent protein (GFP) and GDAP1 or GDAP1$^{p.R120W}$ fused to mCherry has no effect on SOCE activity compared with both empty vectors and with the combination of JPH1 and GDAP1. In contrast, when we overexpress JPH1 and GDAP1$^{p.R120W}$, SOCE activity is lower than in JPH1$^{p.R213P}$ and GDAP1 (Fig. 7C). JPH1$^{p.R213P}$, together with GDAP1$^{p.R120W}$, produces an even lower SOCE activity compared with JPH1 and GDAP1$^{p.R120W}$. The quantification of the SOCE amplitude confirms these observations (Fig. 7D). Thus, it seems that both proteins affect SOCE activity and Ca^{2+} management and that mutations in both could modify the phenotype of cell lines. This SOCE defect is also observed in cells lacking *GDAP1* when both mutations are introduced (Supplementary Material, Fig. S7).

DISCUSSION

The clinical manifestations of the forms caused by *GDAP1* mutations transmitted in an autosomal dominant manner usually show relevant variable expression (6,7). Modifier genes that affect disease severity have been reported for several disorders (29–33) and also systematic analyses of CMT genes have revealed isolated patients who presented a more severe clinical picture because these patients carry mutations in more than one CMT gene (34–37). We have investigated *JPH1* as a candidate modifier gene of *GDAP1* biology because both genes lie close on the same chromosome and are functionally related.

Non-random gene order has been observed in eukaryotic species. It seems likely that conserved organization, which

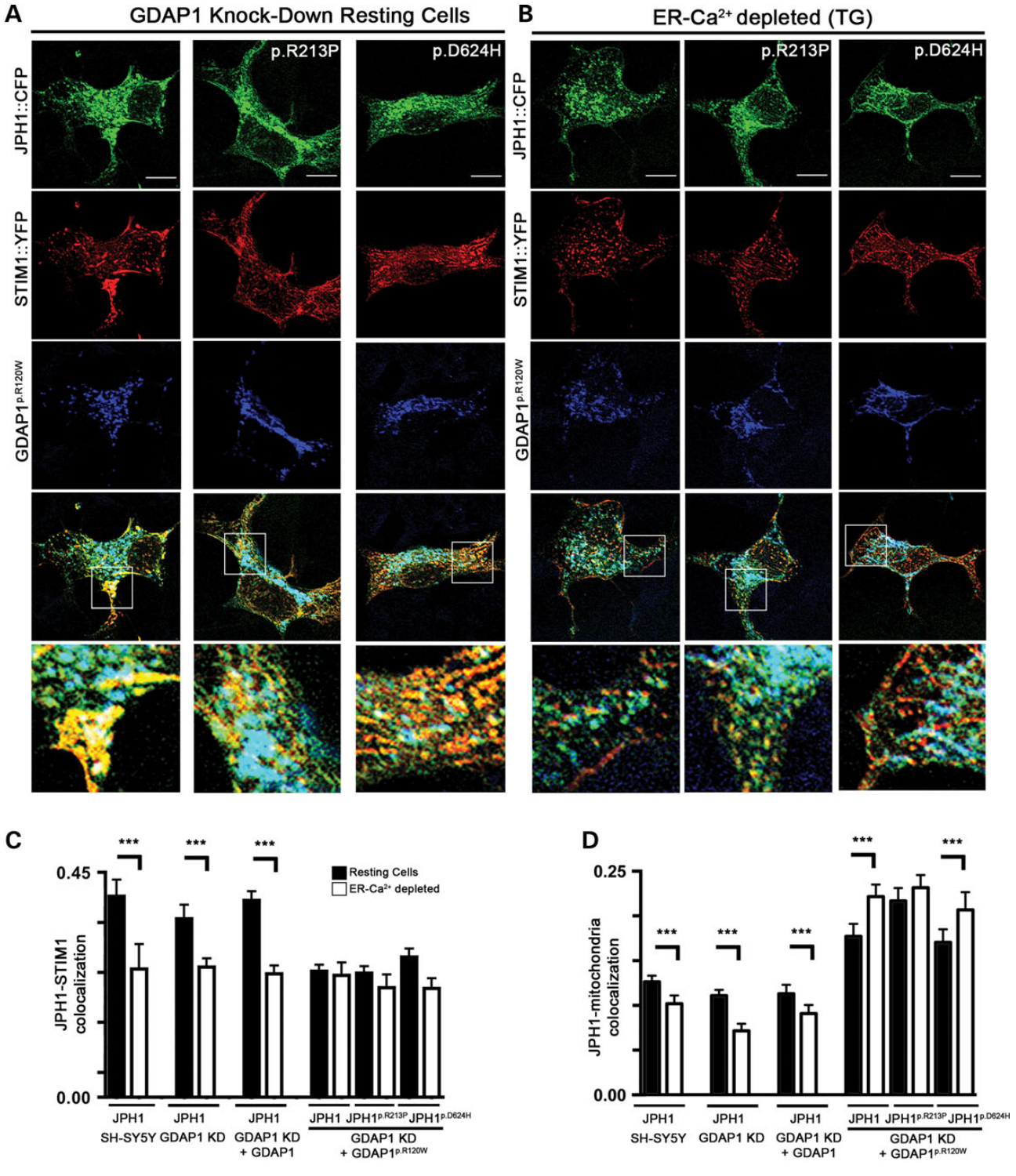

Figure 6. The dominant mutation GDAP1$^{p.R120W}$ produces JPH1 sequestration in mitochondria during ER-Ca^{2+} release. (**A**) Immunofluorescence of *GDAP1* KD cells overexpressing CFP-tagged JPH1 WT, JPH1$^{p.R213P}$ or JPH1$^{p.D624H}$ (green signal), STIM1-YFP (red signal) and myc-tagged GDAP1$^{p.R120W}$ (blue signal) under resting conditions or (**B**) after TG-induced conditions. ER-Ca^{2+} release was induced by adding 5 μM TG in 30 mM D-glucose Ca^{2+}-free HCSS buffer for 10 min before fixation. An enlargement of the boxed region in the merge images is also shown. Scale bar represents 10 μm. (**C**) Quantification of the colocalization measured by Manders'coefficient between JPH1 and STIM1 and (**D**) JPH1 and mitochondria under resting conditions (black bars) or TG-induced conditions (white bars).

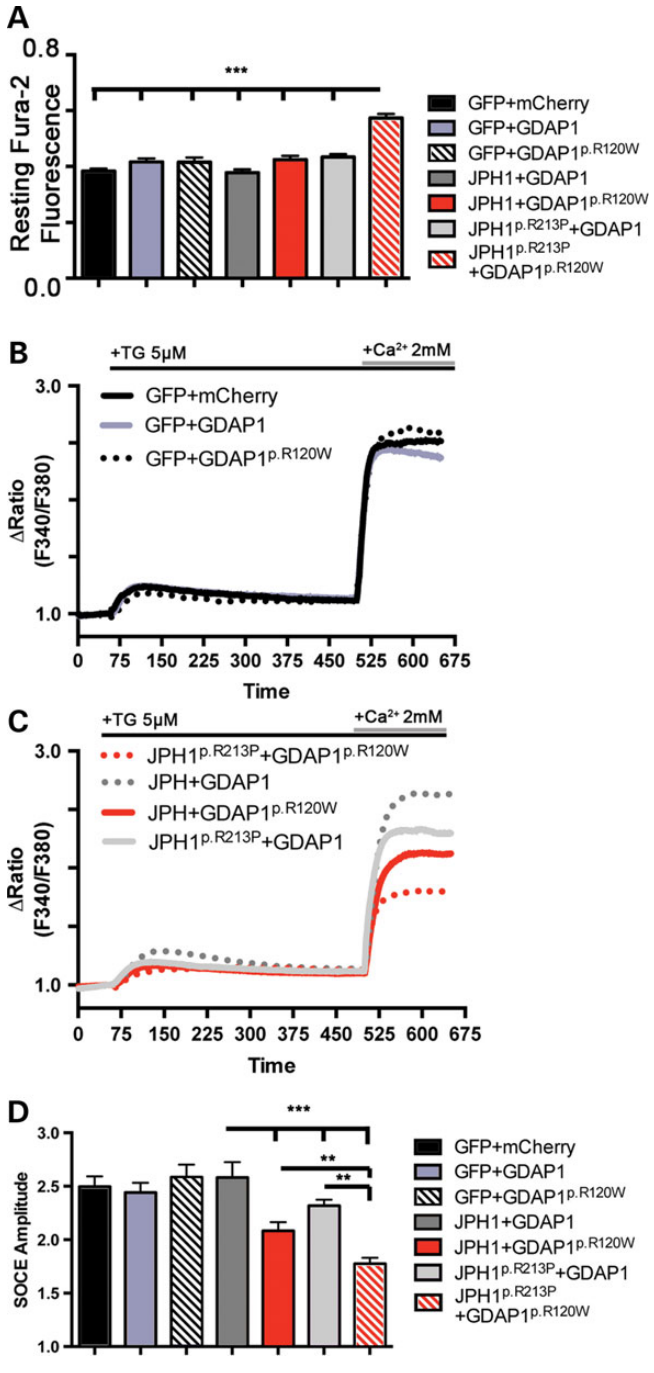

Figure 7. SOCE is blocked by the combination of GDAP1$^{p.R120W}$ and JPH1$^{p.R213P}$. (**A**) Analysis of basal cytosolic Ca^{2+} in SH-SY5Y cells overexpressing the bicistronic pCAGIG plasmid carrying the WT JPH1 or JPH1$^{p.R213P}$ and mCherry-tagged construct of WT GDAP1or GDAP1$^{p.R120W}$ revealed a significant increase when JPH1$^{p.R213P}$ and GDAP1$^{p.R120W}$ are coexpressed. (**B**) Analysis of SOCE combining the pCAGIG empty vector with the mCherry empty vector, mCherry-tagged WT GDAP1 or GDAP1$^{p.R120W}$ showed no effect in SOCE amplitude. (**C**) Analysis of SOCE combining WT JPH1 or JPH1$^{p.R213P}$ with WT GDAP1 or GDAP1$^{p.R120W}$ showed the lowest SOCE response when JPH1$^{p.R213P}$ and GDAP1$^{p.R120W}$ are coexpressed. ER-Ca^{2+} release was induced by adding 5 μM TG before the addition of 2 mM $CaCl_2$ to induce SOCE. (**D**) Comparison of SOCE amplitudes from SOCE analysis (B and C). One-way ANOVA, Tukey's multiple comparison test: $^{*}P < 0.05$; $^{**}P < 0.01$; $^{***}P < 0.001$. Error bars represent the SEM.

refers to genomic position, gene orientation and intergenic distance, may be due to functional relatedness and/or to coordinated expression (19). Using comparative genomics, we established that the *JPH1-GDAP1* and *JPH2-GDAP1L1* blocks constitute a highly conserved paralogon in vertebrates. A common evolutionary origin has been postulated for the *GDAP1*-class genes, suggesting that these genes may have originated extremely early in eukaryotes (8), whereas the *GDAP1L1* arose by gene duplication in the vertebrate lineage. In the same manner, JPHs are highly evolutionarily conserved, and the divergence of JPH into four genes occurred before vertebrates arose (24). The genes that are functionally related, such as participating in the same pathway, tend to be clustered in eukaryotic genomes (22). *GDAP1*, *JPH1* and *JPH2* play roles in Ca^{2+} homeostasis, and the suppression of these genes leads to abnormal SOCE processes (12,17). The function of *GDAP1L1* remains elusive. In *Gdap1*$^{-/-}$ mice, *GDAP1* has been related to the redox response, and *GDAP1L1* has been proposed to compensate for the loss of *GDAP1* in the central nervous system (38). However, the possible implication of *GDADP1L1* in Ca^{2+} metabolism has never been documented.

To identify modifiers of disease severity, those families with dominant *GDAP1* mutations are of particular interest, as shown by the fact that these patients display incomplete penetrance, suggesting that certain carriers develop neurological signs, whereas other carriers reveal minor symptoms after clinical examination (6,7). Thus far, the most frequent dominant mutation detected in the *GDAP1* gene is the p.R120W amino acid change, which is relatively common in Spanish CMT patients and for which a founder effect has been postulated in Spanish population (6,39). In the three investigated families, the *GDAP1* p.R120W mutation and *JPH1* mutations are *in trans*. Clinical features of fCMT-213 and fCMT-214 families have been previously described by Sivera *et al.* (6). In both families, patients with the *JPH1* p.D624H mutation, in addition to the *GDAP1* p.R120W mutation, have been detected. The clinical divergence observed in fCMT-213 and fCMT-214 families cannot be understood by the influence of the *JPH1* p.D624H mutation, which was predicted as a benign polymorphism and, as we have demonstrated in this work, does not alter the function of JPH1. These data suggest that the *JPH1* gene cannot be the only modulator of the disease phenotype in *GDAP1*-related neuropathies.

The proband from the fCMT-408 family is a carrier of the *GDAP1* p.R120W mutation inherited from her father, who is a CMT patient, and of the *JPH1* p.R213P mutation transmitted from her mother, who is a healthy woman. The entire coding regions of the *MFN2*, *HSP22* and *HSP27* genes were analysed in the proband's DNA, and no mutation was found (data not shown). She suffers from a more severe clinical condition compared with her father and her uncles, who are carriers of the *GDAP1* p.R120W mutation. The proband showed a well-defined sensory motor polyneuropathy, whereas the proband's father (ID no. II:4) and his two brothers (ID no. II:1 and II:2) are mildly affected. The almost exclusive affectation of posterior calf muscles in the proband is an intriguing feature. Our other patients with the p.R120W mutation (previously described by Sivera *et al.* (6)) presented a similar grade of weakness on the anterior and posterior calf muscles; however, these patients were older

than this patient, and in two of these patients with a milder phenotype, the MRI showed fatty infiltration only in the superficial posterior calf compartment. These features suggest that weakness might start on posterior muscles of the calves in the *GDAP1* p.R120W patients in contrast to most of CMT patients, who show an earlier and frequent ankle dorsiflexion weakness.

Sural nerve biopsy of the proband presents hypomyelinated axons and significant hypertrophic changes with frequent OB formations, which would correspond to a demyelinating phenomenon although the nerve conduction velocities are clearly in the axonal range. Demyelinating, hypertrophic and axonal features have been described in patients with axonal mitochondrial neuropathies, including *GDAP1* cases (40,41). In previous GDAP1 cases, OB formations were quantitatively less frequent and primarily related to regenerating clusters (6) whereas in this case, the hypertrophic changes were extremely prominent and diffuse. We have observed typical OBs that displayed up to three concentrically arranged Schwann cell processes around a central hypomyelinated axon. Nevertheless, these OBs differ from the classic OBs described in demyelinating CMT in the thickness and number of these cell processes. Taken together, these findings reinforce the previously reported data and broaden the spectrum of neuropathological findings described in patients with the *GDAP1* p.R120W mutation.

The characterization of *JPH1* nucleotide variants in carriers of the *GDAP1* p.R120W led us to investigate whether *JPH1* could be a modifier of *GDAP1* because both proteins are linked to Ca^{2+} homeostasis. GDAP1 is primarily expressed in neurons (10,11), whereas *JPH1* is predominantly expressed in skeletal muscle (13). We have corroborated *JPH1* expression in skeletal muscle and cells and demonstrated its expression in neuronal tissues and cells. These findings allowed us to place both proteins in the same tissues, which is essential if JPH1 and GDAP1 interact with each other in some way. The depletion of *GDAP1* in SH-SY5Y cells results in decreased SOCE activity (12), and *JPH1* expression silencing *in vitro* also decreased SOCE activity (17). The slight differences observed for $JPH1^{p.R213P}$ in the basal cytosolic Ca^{2+} in control cells may not be relevant, because we have shown that JPH1, $JPH1^{p.D624H}$ and $JPH1^{p.R213P}$ present normal SOCE activity in SH-SY5Y cells. Although in *GDAP1* KD cells, only JPH1 and $JPH1^{p.D624H}$ can restore SOCE activity, suggesting that p.R213P alters the proper function of JPH1 in the absence of GDAP1. Furthermore, when a total discharge of Ca^{2+} from the ER and other minor stores is caused by ionomycin in cells lacking *GDAP1*, then the Ca^{2+} content cannot be restored with the expression of $JPH1^{p.R213P}$ or GDAP1. This finding confirms that $JPH1^{p.R213P}$ would require GDAP1 to properly function and would indicate that JPH1 and GDAP1 function in different processes. In fact, the role of GDAP1 in SOCE activity is related to mitochondrial relocation after ER-Ca^{2+} release (12), and we have observed that the restoration of SOCE activity by JPH1 is not associated with a mitochondrial buffer capacity related to mitochondria relocation because SOCE activity in JPH1-overexpressing cells was no longer inhibited by mitochondrial blockers. Thus, the role of JPH1 has been associated with stabilizing SOC channels directly related to refill the ER after SOCE (13,17). *JPH1* knock-out (KO) myotubes present a notable reduction in SOCE presumably caused by physical alteration of SR and T-tubule junctions (42). In an identical manner, the disruption of Ca^{2+} homeostasis has been associated with altered cross talk among Ca^{2+} channels on the T-tubule and SR membranes in the $JPH2^{p.S165F}$-expressing skeletal myotubes (43) and with ultrastructural defects of the ER and mitochondria in cardiac myocytes from *JPH2* KO embryos (13). In summary, JPH1 could act as a structural protein at ER–PM sites during SOCE, and an anomalous JPH1 could abolish SOCE due to the instability of these contact sites.

GDAP1 is an outer mitochondrial membrane protein, whereas JPH1 is primarily at the ER; however, in addition, we have established that both proteins share localization in MAMs, which consist of the ER and become reversibly tethered to mitochondria. These structures are crucial to the proper function of the cell, playing roles in not only lipid metabolism, ER–mitochondria Ca^{2+} fluxes and peroxisome formation but also regulation of the morphology, dynamics and functions of mitochondria (44). Mitochondria are strategically close to the ER and, thereby, are exposed to a high local [Ca^{2+}] during the Ca^{2+} release process. MFN2, which is enriched at MAMs, bridges mitochondria to the ER and forms a juxtaposition required for efficient mitochondrial Ca^{2+} uptake (45,46). Mfn2 silencing in mice fibroblasts disrupts SR morphology, and the efficiency of mitochondrial function is reduced (47). Silencing of JPH2 in embryonic stem cell-derived cardiomyocytes causes an abnormal Ca^{2+} transient, and the juxtaposition of mitochondria with SR is destroyed (48). Increasing evidence emphasizes that MAMs are essential for intercommunications during Ca^{2+} signalling because these structures provide a physical basis (46,49,50).

Our findings indicated that JPH1 forms puncta and colocalizes with STIM1, which is the activator of SOCE, during ER-Ca^{2+} release. STIM1 oligomerizes, migrates to the ER–PM junctions (25,51,52) and colocalizes with Orai1, which is accumulated at PM sites directly opposite STIM1 (26,27). However, $JPH1^{p.R213P}$ seems to have some problems in oligomerization in control cells and during ER-Ca^{2+} release, $JPH1^{p.R213P}$ loses the proper JPH1-STIM1 colocalization in ER–PM puncta structures and shows a higher colocalization with mitochondria in *GDAP1* KD cells, suggesting that a defect in STIM1 oligomerization and migration exists. When GDAP1 is included, the expected pattern is restored, emphasizing that JPH1 activity is GDAP1-dependent. We demonstrated that GDAP1 does not physically interact with JPH1. How GDAP1 is able to modify the JPH1 pattern remains unknown.

The dependence on GDAP1 was more evident with $GDAP1^{p.R120W}$. The colocalization of JPH1 with STIM1 is practically identical under resting conditions or during ER-Ca^{2+} release in the presence of $GDAP1^{p.R120W}$; STIM1 also seems to be more aggregated. In contrast, $JPH1^{p.R213P}$ colocalization with mitochondria is increased under resting conditions, and $GDAP1^{p.R120W}$ retains the WT and mutated JPH1 forms in mitochondria during ER-Ca^{2+} release. The sustained retention of $JPH1^{p.R213P}$ in mitochondria in the presence of $GDAP1^{p.R120W}$ must prevent the proper function of JPH1, and in fact, the lowest SOCE activity was obtained when $GDAP1^{p.R120W}$ and $JPH1^{p.R213P}$ coexisted. GDAP1 functions in mitochondria relocation because mitochondria must be strategically localized near the PM in the proximity of SOCE channels to allow SOCE-Ca^{2+} buffering by mitochondria (12,52). Mitochondria are associated with the ER via tethers that link the outer mitochondrial membrane to the intracellular Ca^{2+} stores and that provide a structural framework for bidirectional signalling between the two organelles (53). Mitochondrial depolarization

selectively regulates STIM1 multimer trafficking to the PM in a MFN2-dependent manner, and a regulatory role for MFN2 in the STIM1 movement has been postulated (54). It is tempting to speculate that GDAP1 could have also a regulatory role related to STIM1 migration, similar to MFN2. These three proteins have closely related functions in mitochondrial dynamics. Mitochondrial fission and fusion cycles are required for neuronal function, and because of these cycles, mitochondria have distinct shapes ranging from tubular to fragmented. In STIM1 KO cells, mitochondria are more tubular and are more densely packed, suggesting that STIM1 is implicated in mitochondrial shape regulation (55). GDAP1 and MFN2 have been related to mitochondria fission and to mitochondria fusion, respectively, and both proteins are in the mitochondrial outer membrane (56).

The basal cytosolic Ca^{2+} level revealed a significant increase when JPH1$^{p.R213P}$ and GDAP1$^{p.R120W}$ are coexpressed. The gain of toxicity due to an increased Ca^{2+} influx has been widely linked with neurodegeneration; thus, intracellular hypercalcaemia is a common pathway for the pathogenesis of several diseases (57), i.e. axonal CMT neuropathies caused by mutations in the *TRPV4* gene (58). The precise mechanism by which the coexistence of both mutations, GDAP1$^{p.R120W}$ and JPH1$^{p.R213P}$, worsen the SOCE response is unclear; however, this combination resembles a *GDAP1* KD phenotype. Supplementary Material, Figure S8 illustrates the effect caused by the presence of the two mutations: the proper localization of JPH1$^{p.R213P}$ is altered in the presence of GDAP1$^{p.R120W}$ causing a dysregulation of the Ca^{2+} fluxes. *JPH1* has not yet been associated with human diseases; nevertheless, aberrant JPH1 proteolysis was identified in a murine model of muscular dystrophy, providing an association with the development of primary muscle disease (59). Heterozygous mutations in *GDAP1* or in the *MFN2* gene cause CMT disease (5,60), and heterozygous mutations in both genes in one patient led to a more severe neuropathy, suggesting cumulative effects (35). The *JPH1* p.R213P mutation alone does not result in symptoms, although this variant seems to act as a negative modifier of the *GDAP1* p.R120W mutation and to lead to a more severe clinical picture, which is closer to autosomal recessive forms of CMT caused by mutations in *GDAP1*. Further work will be required to establish the precise mechanisms involved in Ca^{2+} dysregulation that lead to neurodegeneration and to identify additional genetic factors that may modulate the disease phenotype to completely explain the variable clinical expression.

MATERIALS AND METHODS

Patients

We have investigated a clinically well characterized series of 24 patients that are carriers of the *GDAP1* p.R120W (c.358C>T) mutation and that belong to eight unrelated Spanish families, in which the disease was inherited as an autosomal dominant trait. Clinical pictures of five of these families have been previously described (5,6,39).

Ethics statement

All protocols performed in this study complied with the ethics guidelines in accordance with the tenets of the Declaration of Helsinki and were approved by the institutional review boards (IRBs) of the participating institutions. All patients and relatives were aware of the investigative nature of the studies and gave their consent.

Nerve biopsy

Sural nerve biopsy was performed on the proband. Semi-thin sections stained with toluidine blue were prepared for evaluation under a light microscope as previously described (41). Ultra-thin cut samples were contrasted with uranyl acetate and with lead citrate for ultrastructural study.

Genetic analysis

A search for nucleotide variants in the genomic DNA was performed by Sanger sequencing of the polymerase chain reaction (PCR) products of all the coding exons and their intronic flanking sequences in the *JPH1* gene (Ref Seq: NM_020647.2) in an ABI Prism 3130xl autoanalyser (Applied Biosystems, Foster City, CA, USA). Primers and PCR conditions are available upon request. Sequence-based predictions of the protein consequences of the identified nucleotide variants were assessed using both SIFT (61) and PolyPhen-2 (62) software.

Comparative genomics

To compare the *GDAP1* and the *GDAP1L1* genomic contexts, the following representative vertebrate organisms were selected: *Homo sapiens*, *Mus musculus*, *Gallus gallus*, *Anolis carolinensis*, *Xenopus tropicalis* and *Danio rerio*. Information concerning predicted orthologues and genomic architecture were obtained from NCBI (http://www.ncbi.nlm.nih.gov/). The selected orthologues (Supplementary Material, Table S1 and S2) were confirmed by BLAST searches and by comparison with the human *GDAP1* and *GDAP1L1* genomic contexts.

Constructs and mutagenesis

Human *JPH1* (IMAGE 9021744) and mouse *Jph1* (IMAGE 40129762) were subcloned into the bicistronic pCAGIG plasmid (kindly provided by Dr N. Flames). Human *JPH1* was PCR amplified and subcloned into pEGFP-N1 and pECFP-C1. The *JPH1*$^{p.R213P}$ and *JPH1*$^{p.D624H}$ variants were obtained by PCR-based site-directed mutagenesis (Agilent Technologies, Santa Clara, CA, USA). The *GDAP1*-myc WT and p.R120W mutant constructs were described previously by Pla-Martín *et al*. (12). Human WT *GDAP1* and *GDAP1* p.R120W were subcloned into the pCAGIG plasmid and into the pCDNA3-mCherry plasmid (generated in this work). Human STIM1-CFP, STIM1-YFP and Orai1-CFP plasmids were a gift from Dr J. Satrústegui. Primers used for cloning are listed in the Supplementary Material, Table S3, and detailed information is available in the Supplementary Information.

Cell culture, transfection and immunofluorescence

SH-SY5Y cells were grown in DMEM-F12 (Sigma-Aldrich, St. Louis, MO, USA) supplemented with 10% (v/v) inactivated foetal bovine serum, 2 mM glutamine and 100 mg/ml penicillin–

streptomycin (Invitrogen, Carlsbad, CA, USA). The *GDAP1* KD G4 and pLKO.1-NT stable cell lines described by Pla-Martin *et al*. (12) were maintained in supplemented DMEM-F12 plus 2 μg/ml puromycin (Sigma-Aldrich, St. Louis, MO, USA). HeLa (ECACC no. 93021013), SW10 mouse Schwann cell lines (ATCC number CRL-2766) and human fibroblasts (kindly provided by Dr J. Torres) were grown in DMEM medium (Sigma-Aldrich, St. Louis, MO, USA) supplemented with 10% inactivated (v/v) foetal bovine serum, 2 mM glutamine, 100 U/ml penicillin and 100 μg/ml streptomycin (Invitrogen, Carlsbad, CA, USA), and for the rhabdomyosarcoma RD cell line (ECACC no. 85111502), media were supplemented with 2% vitamins (Sigma-Aldrich, St. Louis, MO, USA) and 2% non-essential amino acids (Sigma-Aldrich, St. Louis, MO, USA). Primary motor neuron cultures were prepared from mouse 12.5-day embryo (E12.5) spinal cords as described previously (63).

For immunofluorescence assays, cells were seeded on glass coverslips and transfected using FuGENE HD (Promega, Madison, WI, USA) following the manufacturer's instructions. The level of transfection was adjusted to obtain the same amount of overexpressed protein in each experiment (Supplementary Material, Fig. S2). ER-Ca^{2+} depletion was performed by washing cells with phosphate-buffered saline (PBS) and by adding 5 μM TG (Alomone Labs, Jerusalem, Israel) in 30 mM D-glucose Ca^{2+}-free HEPES-buffered controlled salt solution (HCSS) buffer (120 mM NaCl, 0.8 mM $MgCl_2$, 25 mM HEPES, and 5.4 mM KCl, pH 7.4) for 10 min. Then, resting and induced cells were fixed for 10 min each using 2 and 4% paraformaldehyde in PBS. Cells were permeabilized with 0.2% Triton X-100 in PBS for 30 min at room temperature, blocked and probed with primary antibodies. α-GRP94 (Abcam, Cambridge, UK), which is an ER marker, α-Cyt *c* (Zymed, Invitrogen, Carlsbad, CA, USA), which is a mitochondrial marker, and α-myc (Sigma-Aldrich, St. Louis, MO, USA) were used to detect GDAP1 or $GDAP1^{p.R120W}$ transfected proteins.

Primary antibodies were detected using goat anti-mouse or goat anti-rabbit antibodies coupled to Alexa Fluor 488 or Alexa Fluor 633 (Molecular Probes, Invitrogen, Carlsbad, CA, USA). Samples were examined using a Leica TCS SP2 confocal system and analysed with the public domain ImageJ program (developed by National Institutes of Health, Bethesda, MD, USA).

For analysing colocalization, a representative stack of the cell was acquired for at least 20 cells and replicated three times for each condition. Then, images were deconvolved, automatically thresholded and analysed using the JACoP ImageJ plugin to obtain Manders' coefficient (64). Manders' coefficient measures the portion of the signal in each channel that coincides with some signals in the other channel.

Reverse transcriptase PCR

Total RNA from 9-month-old mouse tissues was extracted with TriPure isolation reagent (Roche Applied Science, Mannheim, Germany) according to the manufacturer's instructions. Total RNAs from mouse SW10 Schwann cell lines and primary motor neuron cultures (24 and 48 h after plating) were isolated using an RNeasy Mini Kit (Qiagen, Valencia, CA, USA). cDNA was synthesized using M-MLV reverse transcriptase (Invitrogen, Carlsbad, CA, USA). The resulting cDNA was amplified using specific primers for the murine *Jph1* (mJph1-F caattgaaggtgcacaaagg, mJph1-R agcatcagcttttgctctgg) and the *Gapdh* housekeeping gene (Gapdh-F cattgacctcaactacatgg, Gapdh-R caaagttgtcatggatgacc). PCR products were separated on 2% agarose gels.

Immunoblot analysis

Tissue extracts from post-natal 2-month-old mice were homogenized using a polytron homogenizer in lysis buffer (50 mM Tris–HCl, pH 7.4, 1.5 mM $MgCl_2$, 5 mM EDTA, 1% Triton X-100, 1 mM DTT, 50 mM NaF, 1 mM Na_2VO_3, 0.1 mM PMSF and protease inhibitor mixture tablets; Roche Applied Science, Mannheim, Germany). Cardiac and skeletal muscle tissues were ground with a mortar in liquid nitrogen before polytron homogenization. Dorsal root ganglion (DRG) and sciatic nerve homogenates were sonicated for 10 s on ice. Homogenates were clarified by centrifugation at 15 000 *g* for 15 min at 4°C. Protein concentrations were determined using a BCA protein assay kit (Pierce, Thermo Scientific, Rockford, IL, USA). All lysates were resolved on sodium dodecyl sulphate-polyacrylamide gel electrophoresis (SDS-PAGE) and analysed by WB with specific antibodies.

MAMs were isolated as described previously (65). Briefly, two adult mouse brains were homogenized following differential centrifugation steps to separate different organelles. Once mitochondrial fractions were obtained, a sucrose gradient was performed to separate other membrane contaminations. Finally, a Percoll gradient was used to separate mitochondria and MAMs. Fractions were solubilized in SDS-PAGE buffer for further analysis by WB.

The following antibodies were used for immunoblotting: α-JPH1 (Abcam, Cambridge, UK), α-actin (Sigma-Aldrich, St. Louis, MO, USA), α-FACL-4 (Cell Signalling, Beverly, MA, USA) as a MAMs marker, α-Cyt *c* (BD Pharmingen, San José, CA, USA) as a mitochondrial marker and α-GDAP1 (Abnova, Taipei, Taiwan).

Measurement of $[Ca^{2+}]_{cyt}$

Cytosolic Ca^{2+} imaging with Fura-2 was performed as described by Ruiz *et al*. (66). Briefly, cells were plated onto 24 mm round coverslips, transfected with plasmids as described previously, loaded with Fura-2AM by incubation in 30 mM D-glucose Ca^{2+}-free HCSS with 5 μM Fura-2AM and 50 μM pluronic F-127 acid (Sigma-Aldrich, St. Louis, MO, USA) for 30 min at 37°C and, finally, rinsed with HCSS and 2 mM $CaCl_2$, for 30 min. Regions of interest (ROIs) were selected covering single- or double-transfected cells. The fluorescence (emission = 510 nm) ratio of Ca^{2+}-free (F380) to Ca^{2+}-bound probe (F340) was analysed using Metafluor for Leica developed by Metamorph (Universal Imaging). Cells transfected with empty vectors were used as controls in each condition. To compare the different proteins, all values were normalized to the basal ratio.

SOCE analysis was performed using a standard protocol, depleting ER-Ca^{2+} using 5 μM of TG in HCSS-Ca^{2+} free media and inducing SOCE with 2 mM of $CaCl_2$. More than 50 transfected cells were analysed in at least five independent experiments. ER-Ca^{2+} content analysis was performed by inducing cells with 5 μM of ionophore A23187 (Sigma-Aldrich, St. Louis, MO, USA) in HCSS-Ca^{2+}-free media with 1 mM EGTA. To address the dependence of mitochondria in JPH1-

overexpressed cells, we performed a standard SOCE protocol after blocking mitochondria with antimycin A (5 μg/ml) and oligomycin (0.5 μg/ml) (Sigma-Aldrich, St. Louis, MO, USA).

SUPPLEMENTARY MATERIAL

Supplementary Material is available at *HMG* online.

ACKNOWLEDGEMENTS

We thank the proband and her relatives for their kind collaboration. We are grateful to José Conejos-Vila for his technical assistance and Antonio Marco for his recommendations related to comparative genomics. We are also grateful to Dr Jorgina Satrústegui for reviewing the manuscript and for her encouragement during this project. The English text was revised by American Journal Experts.

Conflict of Interest statement. None declared.

FUNDING

This work was supported by the IRDiRC and funded by the Instituto de Salud Carlos III (ISCIII)—Subdirección General de Evaluación y Fomento de la Investigación within the framework of the National R+D+I Plan (Grants no. IR11/TREAT-CMT and PI12/00453), cofunded with FEDER funds, and Ministry of Economy and Competitiveness (Grant no. SAF2012-32425). C.E. has a 'Miguel Servet' contract funded by the ISCIII and Centro de Investigación Biomédica en Red de Enfermedades Raras (CIBERER) (Grant no. CP08/00053). E.C. has a FPU grant funded by the Ministerio de Educación (Grant no. AP2009-0642). The CIBERER is an initiative from the ISCIII.

REFERENCES

1. Baxter, R.V., Ben Othmane, K., Rochelle, J.M., Stajich, J.E., Hulette, C., Dew-Knight, S., Hentati, F., Ben Hamida, M., Bel, S., Stenger, J.E. *et al.* (2002) Ganglioside-induced differentiation-associated protein-1 is mutant in Charcot–Marie–Tooth disease type 4A/8q21. *Nat. Genet.*, **30**, 21–22.
2. Cuesta, A., Pedrola, L., Sevilla, T., Garcia-Planells, J., Chumillas, M.J., Mayordomo, F., LeGuern, E., Marin, I., Vilchez, J.J. and Palau, F. (2002) The gene encoding ganglioside-induced differentiation-associated protein 1 is mutated in axonal Charcot–Marie–Tooth type 4A disease. *Nat. Genet.*, **30**, 22–25.
3. Nelis, E., Erdem, S., Van Den Bergh, P.Y., Belpaire-Dethiou, M.C., Ceuterick, C., Van Gerwen, V., Cuesta, A., Pedrola, L., Palau, F., Gabreels-Festen, A.A. *et al.* (2002) Mutations in GDAP1: autosomal recessive CMT with demyelination and axonopathy. *Neurology*, **59**, 1865–1872.
4. Senderek, J., Bergmann, C., Ramaekers, V.T., Nelis, E., Bernert, G., Makowski, A., Zuchner, S., De Jonghe, P., Rudnik-Schoneborn, S., Zerres, K. *et al.* (2003) Mutations in the ganglioside-induced differentiation-associated protein-1 (GDAP1) gene in intermediate type autosomal recessive Charcot–Marie–Tooth neuropathy. *Brain*, **126**, 642–649.
5. Claramunt, R., Pedrola, L., Sevilla, T., Lopez de Munain, A., Berciano, J., Cuesta, A., Sanchez-Navarro, B., Millan, J.M., Saifi, G.M., Lupski, J.R. *et al.* (2005) Genetics of Charcot–Marie–Tooth disease type 4A: mutations, inheritance, phenotypic variability, and founder effect. *J. Med. Genet.*, **42**, 358–365.
6. Sivera, R., Espinós, C., Vilchez, J.J., Mas, F., Martinez-Rubio, D., Chumillas, M.J., Mayordomo, F., Muelas, N., Bataller, L., Palau, F. *et al.* (2010) Phenotypical features of the p.R120W mutation in the GDAP1 gene causing autosomal dominant Charcot–Marie–Tooth disease. *J. Peripher. Nerv. Syst.*, **15**, 334–344.
7. Zimon, M., Baets, J., Fabrizi, G.M., Jaakkola, E., Kabzinska, D., Pilch, J., Schindler, A.B., Cornblath, D.R., Fischbeck, K.H., Auer-Grumbach, M. *et al.* (2011) Dominant GDAP1 mutations cause predominantly mild CMT phenotypes. *Neurology*, **77**, 540–548.
8. Marco, A., Cuesta, A., Pedrola, L., Palau, F. and Marín, I. (2004) Evolutionary and structural analyses of GDAP1, involved in Charcot–Marie–Tooth disease, characterize a novel class of glutathione transferase-related genes. *Mol. Biol. Evol.*, **21**, 176–187.
9. Pedrola, L., Espert, A., Wu, X., Claramunt, R., Shy, M.E. and Palau, F. (2005) GDAP1, the protein causing Charcot–Marie–Tooth disease type 4A, is expressed in neurons and is associated with mitochondria. *Hum. Mol. Genet.*, **14**, 1087–1094.
10. Niemann, A., Ruegg, M., La Padula, V., Schenone, A. and Suter, U. (2005) Ganglioside-induced differentiation associated protein 1 is a regulator of the mitochondrial network: new implications for Charcot–Marie–Tooth disease. *J. Cell. Biol.*, **70**, 1067–1078.
11. Pedrola, L., Espert, A., Valdes-Sanchez, T., Sanchez-Piris, M., Sirkowski, E.E., Scherer, S.S., Farinas, I. and Palau, F. (2008) Cell expression of GDAP1 in the nervous system and pathogenesis of Charcot–Marie–Tooth type 4A disease. *J. Cell. Mol. Med.*, **12**, 679–689.
12. Pla-Martín, D., Rueda, C.B., Estela, A., Sánchez-Piris, M., González-Sánchez, P., Traba, J., de la Fuente, S., Scorrano, L., Renau-Piqueras, J., Alvarez, J. *et al.* (2013) Silencing of the Charcot–Marie–Tooth disease-associated gene GDAP1 induces abnormal mitochondrial distribution and affects Ca^{2+} homeostasis by reducing store-operated Ca^{2+} entry. *Neurobiol. Dis.*, **55**, 140–151.
13. Takeshima, H., Komazaki, S., Nishi, M., Iino, M. and Kangawa, K. (2000) Junctophilins: a novel family of junctional membrane complex proteins. *Mol. Cell.*, **6**, 11–22.
14. Lee, M.G., Wynder, C., Bochar, D.A., Hakimi, M.A., Cooch, N. and Shiekhattar, R. (2006) Functional interplay between histone demethylase and deacetylase enzymes. *Mol. Cell. Biol.*, **26**, 6395–6402.
15. Ito, K., Komazaki, S., Sasamoto, K., Yoshida, M., Nishi, M., Kitamura, K. and Takeshima, H. (2001) Deficiency of triad junction and contraction in mutant skeletal muscle lacking junctophilin type 1. *J. Cell. Biol.*, **154**, 1059–1067.
16. Yamazaki, D., Yamazaki, T. and Takeshima, H. (2009) New molecular components supporting ryanodine receptor-mediated Ca(2+) release: roles of junctophilin and TRIC channel in embryonic cardiomyocytes. *Pharmacol. Ther.*, **121**, 265–272.
17. Hirata, Y., Brotto, M., Weisleder, N., Chu, Y., Lin, P., Zhao, X., Thornton, A., Komazaki, S., Takeshima, H., Ma, J. *et al.* (2006) Uncoupling store-operated Ca^{2+} entry and altered Ca^{2+} release from sarcoplasmic reticulum through silencing of junctophilin genes. *Biophys. J.*, **90**, 4418–4427.
18. Ko, J.K., Choi, K.H., Zhao, X., Komazaki, S., Pan, Z., Weisleder, N. and Ma, J. (2011) A versatile single-plasmid system for tissue-specific and inducible control of gene expression in transgenic mice. *FASEB J.*, **25**, 2638–2649.
19. Hurst, L.D., Pal, C. and Lercher, M.J. (2004) The evolutionary dynamics of eukaryotic gene order. *Nat. Rev. Genet.*, **5**, 299–310.
20. Serrano-Candelas, E., Farre, D., Aranguren-Ibanez, A., Martinez-Hoyer, S. and Perez-Riba, M. (2014) The vertebrate RCAN gene family: novel insights into evolution, structure and regulation. *PLoS One*, **9**, e85539.
21. Davila Lopez, M., Martinez Guerra, J.J. and Samuelsson, T. (2010) Analysis of gene order conservation in eukaryotes identifies transcriptionally and functionally linked genes. *PLoS One*, **5**, e10654.
22. Lee, J.M. and Sonnhammer, E.L. (2003) Genomic gene clustering analysis of pathways in eukaryotes. *Genome. Res.*, **13**, 875–882.
23. Nishi, M., Mizushima, A., Nakagawara, K. and Takeshima, H. (2000) Characterization of human junctophilin subtype genes. *Biochem. Biophys. Res. Commun.*, **273**, 920–927.
24. Garbino, A., van Oort, R.J., Dixit, S.S., Landstrom, A.P., Ackerman, M.J. and Wehrens, X.H. (2009) Molecular evolution of the junctophilin gene family. *Physiol. Genomics*, **37**, 175–186.
25. Orci, L., Ravazzola, M., Le Coadic, M., Shen, W.W., Demaurex, N. and Cosson, P. (2009) From the cover: STIM1-induced precortical and cortical subdomains of the endoplasmic reticulum. *Proc. Natl. Acad. Sci. USA*, **106**, 19358–19362.
26. Luik, R.M., Wu, M.M., Buchanan, J. and Lewis, R.S. (2006) The elementary unit of store-operated Ca^{2+} entry: local activation of CRAC channels by STIM1 at ER-plasma membrane junctions. *J. Cell. Biol.*, **174**, 815–825.

27. Xu, P., Lu, J., Li, Z., Yu, X., Chen, L. and Xu, T. (2006) Aggregation of STIM1 underneath the plasma membrane induces clustering of Orai1. *Biochem. Biophys. Res. Commun.*, **350**, 969–976.
28. Kopach, O., Kruglikov, I., Pivneva, T., Voitenko, N., Verkhratsky, A. and Fedirko, N. (2011) Mitochondria adjust Ca(2+) signaling regime to a pattern of stimulation in salivary acinar cells. *Biochim. Biophys. Acta*, **1813**, 1740–1748.
29. Venturini, G., Rose, A.M., Shah, A.Z., Bhattacharya, S.S. and Rivolta, C. (2012) CNOT3 is a modifier of PRPF31 mutations in retinitis pigmentosa with incomplete penetrance. *PLoS Genet.*, **8**, e1003040.
30. Prior, T.W., Krainer, A.R., Hua, Y., Swoboda, K.J., Snyder, P.C., Bridgeman, S.J., Burghes, A.H. and Kissel, J.T. (2009) A positive modifier of spinal muscular atrophy in the SMN2 gene. *Am. J. Hum. Genet.*, **85**, 408–413.
31. Sacconi, S., Lemmers, R.J., Balog, J., van der Vliet, P.J., Lahaut, P., van Nieuwenhuizen, M.P., Straasheijm, K.R., Debipersad, R.D., Vos-Versteeg, M., Salviati, L. *et al.* (2013) The FSHD2 gene SMCHD1 is a modifier of disease severity in families affected by FSHD1. *Am. J. Hum. Genet.*, **93**, 744–751.
32. Brewer, M.H., Ma, K.H., Beecham, G.W., Gopinath, C., Baas, F., Choi, B.O., Reilly, M.M., Shy, M.E., Zuchner, S., Svaren, J. *et al.* (2014) Haplotype-specific modulation of a SOX10/CREB response element at the Charcot–Marie–Tooth disease type 4C locus SH3TC2. *Hum. Mol. Genet.*, **24**, 5171–5187.
33. Lamar, K.-M. and McNally, E.M. (2014) Genetic modifiers for neuromuscular diseases. *J. Neuromuscul. Dis.*, **1**, 3–13.
34. Chung, K.W., Sunwoo, I.N., Kim, S.M., Park, K.D., Kim, W.K., Kim, T.S., Koo, H., Cho, M., Lee, J. and Choi, B.O. (2005) Two missense mutations of EGR2 R359W and GJB1 V136A in a Charcot–Marie–Tooth disease family. *Neurogenetics*, **6**, 159–163.
35. Vital, A., Latour, P., Sole, G., Ferrer, X., Rouanet, M., Tison, F., Vital, C. and Goizet, C. (2012) A French family with Charcot–Marie–Tooth disease related to simultaneous heterozygous MFN2 and GDAP1 mutations. *Neuromuscul. Disord.*, **22**, 735–741.
36. Brozkova, D., Mazanec, R., Haberlova, J., Sakmaryova, I. and Seeman, P. (2010) Clinical and in silico evidence for and against pathogenicity of 11 new mutations in the MPZ gene. *Clin. Genet.*, **78**, 81–87.
37. Cassereau, J., Casasnovas, C., Gueguen, N., Malinge, M.C., Guillet, V., Reynier, P., Bonneau, D., Amati-Bonneau, P., Banchs, I., Volpini, V. *et al.* (2011) Simultaneous MFN2 and GDAP1 mutations cause major mitochondrial defects in a patient with CMT. *Neurology*, **76**, 1524–1526.
38. Niemann, A., Huber, N., Wagner, K.M., Somandin, C., Horn, M., Lebrun-Julien, F., Angst, B., Pereira, J.A., Halfter, H., Welzl, H. *et al.* (2014) The Gdap1 knockout mouse mechanistically links redox control to Charcot–Marie–Tooth disease. *Brain*, **137**, 668–682.
39. Sivera, R., Sevilla, T., Vilchez, J.J., Martinez-Rubio, D., Chumillas, M.J., Vazquez, J.F., Muelas, N., Bataller, L., Millan, J.M., Palau, F. *et al.* (2013) Charcot–Marie–Tooth disease: genetic and clinical spectrum in a Spanish clinical series. *Neurology*, **81**, 1617–1625.
40. Vital, A. and Vital, C. (2012) Mitochondria and peripheral neuropathies. *J. Neuropathol. Exp. Neurol.*, **71**, 1036–1046.
41. Sevilla, T., Cuesta, A., Chumillas, M.J., Mayordomo, F., Pedrola, L., Palau, F. and Vílchez, J.J. (2003) Clinical, electrophysiological and morphological findings of Charcot–Marie–Tooth neuropathy with vocal cord palsy and mutations in the GDAP1 gene. *Brain*, **126**, 2023–2033.
42. Li, H., Ding, X., Lopez, J.R., Takeshima, H., Ma, J., Allen, P.D. and Eltit, J.M. (2010) Impaired Orai1-mediated resting Ca^{2+} entry reduces the cytosolic [Ca^{2+}] and sarcoplasmic reticulum Ca^{2+} loading in quiescent junctophilin 1 knock-out myotubes. *J. Biol. Chem.*, **285**, 39171–39179.
43. Woo, J.S., Hwang, J.H., Ko, J.K., Weisleder, N., Kim do, H., Ma, J. and Lee, E.H. (2010) S165F mutation of junctophilin 2 affects Ca^{2+} signalling in skeletal muscle. *Biochem. J.*, **427**, 125–134.
44. Vance, J.E. (2014) MAM (mitochondria-associated membranes) in mammalian cells: lipids and beyond. *Biochim. Biophys. Acta.*, **1841**, 595–609.
45. Eura, Y., Ishihara, N., Oka, T. and Mihara, K. (2006) Identification of a novel protein that regulates mitochondrial fusion by modulating mitofusin (Mfn) protein function. *J. Cell. Sci.*, **119**, 4913–4925.
46. de Brito, O.M. and Scorrano, L. (2008) Mitofusin 2 tethers endoplasmic reticulum to mitochondria. *Nature*, **456**, 605–610.
47. Chen, H., Detmer, S.A., Ewald, A.J., Griffin, E.E., Fraser, S.E. and Chan, D.C. (2003) Mitofusins Mfn1 and Mfn2 coordinately regulate mitochondrial fusion and are essential for embryonic development. *J. Cell. Biol.*, **160**, 189–200.
48. Liang, X., Mei, Y., Huang, X., Shen, G., Zhu, D., Yu, Y., Wang, J. and Lou, Y. (2012) Junctophilin 2 knockdown interfere with mitochondrium status in ESC-CMs and cardiogenesis of ES cells. *J. Cell. Biochem.*, **113**, 2884–2894.
49. de Brito, O.M. and Scorrano, L. (2009) Mitofusin-2 regulates mitochondrial and endoplasmic reticulum morphology and tethering: the role of Ras. *Mitochondrion*, **9**, 222–226.
50. Parekh, A. (2009) Calcium signalling: mitofusins promote interorganellar crosstalk. *Curr. Biol.*, **19**, R200–R203.
51. Wu, M.M., Buchanan, J., Luik, R.M. and Lewis, R.S. (2006) Ca^{2+} store depletion causes STIM1 to accumulate in ER regions closely associated with the plasma membrane. *J. Cell Biol.*, **174**, 803–813.
52. Lur, G., Haynes, L.P., Prior, I.A., Gerasimenko, O.V., Feske, S., Petersen, O.H., Burgoyne, R.D. and Tepikin, A.V. (2009) Ribosome-free terminals of rough ER allow formation of STIM1 puncta and segregation of STIM1 from IP(3) receptors. *Curr. Biol.*, **19**, 1648–1653.
53. Boncompagni, S., Rossi, A.E., Micaroni, M., Beznoussenko, G.V., Polishchuk, R.S., Dirksen, R.T. and Protasi, F. (2009) Mitochondria are linked to calcium stores in striated muscle by developmentally regulated tethering structures. *Mol. Biol. Cell.*, **20**, 1058–1067.
54. Singaravelu, K., Nelson, C., Bakowski, D., de Brito, O.M., Ng, S.W., Di Capite, J., Powell, T., Scorrano, L. and Parekh, A.B. (2011) Mitofusin 2 regulates STIM1 migration from the Ca^{2+} store to the plasma membrane in cells with depolarized mitochondria. *J. Biol. Chem.*, **286**, 12189–12201.
55. Henke, N., Albrecht, P., Pfeiffer, A., Toutzaris, D., Zanger, K. and Methner, A. (2012) Stromal interaction molecule 1 (STIM1) is involved in the regulation of mitochondrial shape and bioenergetics and plays a role in oxidative stress. *J. Biol. Chem.*, **287**, 42042–42052.
56. Niemann, A., Wagner, K.M., Ruegg, M. and Suter, U. (2009) GDAP1 mutations differ in their effects on mitochondrial dynamics and apoptosis depending on the mode of inheritance. *Neurobiol. Dis.*, **36**, 509–520.
57. Duchen, M.R. (2012) Mitochondria, calcium-dependent neuronal death and neurodegenerative disease. *Pflugers Arch.*, **464**, 111–121.
58. Klein, C.J., Shi, Y., Fecto, F., Donaghy, M., Nicholson, G., McEntagart, M.E., Crosby, A.H., Wu, Y., Lou, H., McEvoy, K.M. *et al.* (2011) TRPV4 mutations and cytotoxic hypercalcemia in axonal Charcot–Marie–Tooth neuropathies. *Neurology*, **76**, 887–894.
59. Murphy, R.M., Dutka, T.L., Horvath, D., Bell, J.R., Delbridge, L.M. and Lamb, G.D. (2013) Ca^{2+}-dependent proteolysis of junctophilin-1 and junctophilin-2 in skeletal and cardiac muscle. *J. Physiol.*, **591**, 719–729.
60. Zuchner, S., Mersiyanova, I.V., Muglia, M., Bissar-Tadmouri, N., Rochelle, J., Dadali, E.L., Zappia, M., Nelis, E., Patitucci, A., Senderek, J. *et al.* (2004) Mutations in the mitochondrial GTPase mitofusin 2 cause Charcot–Marie–Tooth neuropathy type 2A. *Nat. Genet.*, **36**, 449–451.
61. Ng, P.C. and Henikoff, S. (2003) SIFT: predicting amino acid changes that affect protein function. *Nucleic Acids Res.*, **31**, 3812–3814.
62. Adzhubei, I.A., Schmidt, S., Peshkin, L., Ramensky, V.E., Gerasimova, A., Bork, P., Kondrashov, A.S. and Sunyaev, S.R. (2010) A method and server for predicting damaging missense mutations. *Nat. Methods*, **7**, 248–249.
63. Gou-Fabregas, M., Garcera, A., Mincheva, S., Perez-García, M.J., Comella, J.X. and Soler, R.M. (2009) Specific vulnerability of mouse spinal cord motoneurons to membrane depolarization. *J. Neurochem.*, **110**, 1842–1854.
64. Bolte, S. and Cordelieres, F.P. (2006) A guided tour into subcellular colocalization analysis in light microscopy. *J. Microsc.*, **224**, 213–232.
65. Annunziata, I., Patterson, A. and d'Azzo, A. (2013) Mitochondria-associated ER membranes (MAMs) and glycosphingolipid enriched microdomains (GEMs): isolation from mouse brain. *J. Vis. Exp.*, e50215, doi:10.3791/50215.
66. Ruiz, F., Alvarez, G., Pereira, R., Hernandez, M., Villalba, M., Cruz, F., Cerdan, S., Bogonez, E. and Satrústegui, J. (1998) Protection by pyruvate and malate against glutamate-mediated neurotoxicity. *Neuroreport*, **9**, 1277–1282.